INTERNATIONAL JOURNAL OF HYDROGEN ENERGY 45 (2020) 574–594

Available online at www.sciencedirect.com

ScienceDirect

journal homepage: www.elsevier.com/locate/he

Enhancement of ethanol electrooxidation in half cell and single direct ethanol fuel cell (DEFC) using post-treated polyol synthesized Pt-Ru nano electrocatalysts supported on HNO_3-functionalized acetylene black carbon

*Abhay Kumar Choudhary, Hiralal Pramanik**

Department of Chemical Engineering & Technology, Indian Institute of Technology (Banaras Hindu University), Varanasi, U.P., India

HIGHLIGHTS

- Post treatment of Pt-Ru/C_{AB}-syn electrocatalyst improved cell performance significantly.
- HNO_3 functionalized acetylene black C_{AB} proved to be an excellent support material.
- Performance of post treated Pt-Ru/C_{AB}-H_2-RT was comparable to commercial Pt-Ru/C.
- Highest alloying of Ru with Pt for Pt-Ru/C_{AB}-H_2-RT facilitates ethanol splitting.

ARTICLE INFO

Article history:
Received 28 July 2019
Received in revised form
21 October 2019
Accepted 27 October 2019
Available online 27 November 2019

Keywords:
Polyol synthesis
Post treatment
Pt-Ru electrocatalyst
Ethanol electrooxidation
Cyclic voltammetry

ABSTRACT

Highly dispersed Pt-Ru nano electrocatalysts supported on functionalized acetylene black carbon (C_{AB}) were synthesized by a modified polyol reduction route followed by post treatment under three different conditions. The synthesized Pt-Ru/C_{AB}-syn electrocatalysts after post treatment were designated as Pt-Ru/C_{AB}-H_2-RT when treated under H_2 atmosphere at room temperature of 40 °C, and Pt-Ru/C_{AB}-H_2-160 when treated under H_2 atmosphere at 160 °C and Pt-Ru/C_{AB}-Air-160 when treated under air at 160 °C, respectively. The post treatment of synthesized electrocatalyst modified the crystallographic and morphological structures of the synthesized electrocatalysts which enhanced the electrocatalytic activity for ethanol electrooxidation. The physical characteristics of the post-treated electrocatalysts were recorded using XRD, SEM-EDX and TEM techniques. The XRD and TEM analyses revealed that the synthesized electrocatalysts have particle size in nano range with narrow size distribution. The electrochemical study of synthesized electrocatalysts were evaluated via cyclic voltammetry and chronoamperometry revealed that the Pt-Ru/C_{AB}-H_2-RT electrocatalyst is the most active exhibit towards ethanol electrooxidation in comparison to that of Pt-Ru/C_{AB}-H_2-160, Pt-Ru/C_{AB}-Air-160 and commercial Pt-Ru/C electrocatalysts. In DEFC performance test at a temperature of 40 °C, the obtained power density (9.15 mW/cm^2) using the synthesized Pt-Ru/C_{AB}-H_2-RT as anode electrocatalyst was higher than that of Pt-Ru/C_{AB}-Air-160 (5.79 mW/cm^2), Pt-Ru/C_{AB}-H_2-160 (6.84 mW/cm^2) and commercial Pt-Ru/C (7.86 mW/cm^2) electrocatalysts with same anode electrocatalyst loading of 1 mg/cm^2 and 2 M ethanol fuel. The maximum OCV of 0.737 V and power density of 16.23 mW/cm^2 at 0.317 V with a current density of 51.2 mA/cm^2 were

* *Corresponding author.*
E-mail address: hpramanik.che@itbhu.ac.in (H. Pramanik).
https://doi.org/10.1016/j.ijhydene.2019.10.243

obtained using Pt-Ru/C_{AB}-H_2-RT electrocatalyst as anode at a cell temperature of 80 °C. The enhanced and superior performance of Pt-Ru/C_{AB}-H_2-RT electrocatalyst after post treatment could be attributed to well alloyed microstructure and highly dispersed surface morphology of metal nanoparticles.

Introduction

Power generation based on proton exchange membrane (PEM) technology has drawn significant attentions due to its several benefits over other types of fuel cells in the low temperature range [1]. Low temperature fuel cells are operated with anode fuels mostly hydrogen or hydrogen rich molecules like methanol, ethanol, acetic acid, $NaBH_4$, etc [2,3]. These fuels are environmentally friendly and result in high output from fuel cells, silent system and water is the only byproduct for hydrogen fuel [3,4]. In this context, fuel cells represent a promising route for electricity production without any environment pollution and thus obviously have spurred a lot of interest amongst the researchers all over the world [3–5].

Although, hydrogen is considered as a clean energy carrier due to its environmental benignity and high energy density of 39.4 kWh kg^{-1}, some convincing drawbacks of hydrogen fuel such as low volumetric energy density, economical production of pure hydrogen gas, onboard storage and safety issues are the key reasons to go for other liquid fuels rather than hydrogen [3,6]. Among various liquid fuels methanol and ethanol are widely used in proton exchange membrane fuel cells (PEMFCs) in place of hydrogen, which represents the ultimate fuels of the future for sustainable energy supply. Methanol being a liquid fuel has the advantages of easy storage and transportation and thus it could be an alternative fuel for hydrogen in PEMFCs [7]. However, methanol offers cross-over problem which resulting in a mixed potential at cathode, and consequently reduce the fuel cell performance. Moreover, it is produced via chemical route from nonrenewable sources, neurotoxic in nature, volatile and inflammable [4]. On the other hand, ethanol is particularly promising viable liquid fuel that can be commonly used in PEMFCs as ethanol offers several advantages over methanol fuel like higher energy density (8.0 kWh kg^{-1} vs 6.1 kWh kg^{-1}), non-toxic, little higher boiling point than methanol and bulkier than methanol molecule thus less cross-over problem. Moreover, ethanol is renewable in nature and it can be easily produced in large quantities by fermentation process from renewable agricultural biomass sources [8–11]. However, electrooxidation of ethanol using present electrocatalyst is truly challenging task to the researchers due to its complex molecular structure. Thus ethanol was selected as promising fuel for the use in PEM base direct ethanol fuel cells (DEFCs) in the present study.

It is well known that there is still a lack of highly active and selective anode electrocatalysts that can initiate the complete electrooxidation of ethanol to CO_2 and H_2O produces a high yield of 12 electrons per molecule with a faster anode kinetics which limits their potential use in DEFCs [10]. As reported in the literature, the ethanol electrooxidation reaction undergoes both parallel and successive oxidation reactions mechanisms due to the presence of the C-C bond of ethanol molecule having low electron affinity and ionization energy [11]. The breaking of the C-C bond of ethanol is a considerable challenge at low temperatures and thus results in incomplete ethanol electrooxidation to complicated adsorbed intermediates and byproducts such as CH_3CHO and CH_3COOH with a small amount of CO_2 (<1%) [12–15].

A three step reaction scheme has been proposed by Pramanik and Basu [16] and Goel and Basu [17] for ethanol the electrooxidation on PtRu/C electrocatalyst electrodes in acidic medium at moderate temperatures (<100 °C), as follow:

$$CH_3CH_2OH + Pt \rightarrow [CH_3CH_2OH]_{ads,Pt} \rightarrow [CH_3CHO]_{ads,Pt}, + 2H^+ + 2e^- \quad (1)$$

$$H_2O + Ru \rightarrow [OH]_{ads,Ru} + H^+ + e^- \quad (2)$$

$$[CH_3CHO]_{ads,Pt} + [OH]_{ads,Ru} \rightarrow CH_3COOH + H^+ + e^- \quad (3)$$

The ethanol oxidation in DEFC using bimetallic Pt-Ru/C electrocatalyst due to the bifunctional mechanism [10], ethanol molecule first gets adsorbed on the surface of Pt electrocatalyst to form acetaldehyde, and further release proton and electrons (Eq. (1)). According to the second reaction step (Eq. (2)), on the surface of Ru metal of bi-metallic Pt-Ru/C electrocatalyst, a dissociative adsorption of water takes place. The adsorbed species (e.g., $[CH_3CHO]_{ads,Pt}$ and $[OH]_{ads,Ru}$) interacts each other and forms acetic acid (Eq. (3)).

At high potential region [18], the mechanism is expressed by reactions (4) and (5):

$$Pt\text{-}CH_3CHO_{ads} + OH_{ads} \rightarrow Pt + CH_3COOH + H^+ + e^- \quad (4)$$

$$Pt\text{-}CO_{ads} + OH_{ads} \rightarrow Pt + CO_2 + H^+ + e^- \quad (5)$$

Here, the activation H_2O to the OH^- species is rate determining step.

At the beginning of 21st century, platinum was considered as an efficient anode electrocatalyst for ethanol oxidation in acidic medium, as it generated significant current in CV studies in comparison to gold and other metals [2,10]. However, it requires significant activation overpotential and its reaction kinetics rate is rather slow. Moreover, its surface gets poisoned very fast by strongly adsorbed intermediates, which are CO-like intermediate species produced during dissociative adsorption of ethanol [10,11]. In order to overcome the poisoning effect of CO and enhance the electrocatalytic activity of pure Pt towards ethanol electrooxidation, the formation of alloys with second oxophilic metals such as Ru, Sn, Ir, Re, Rh, or Mo have given major emphasis for the last few years [8,19–27]. Among bimetallic electrocatalysts, Pt-Sn and Pt-Ru are most promising due to their better capability to overcome CO poisoning effect in acidic medium [20,21]. The enhanced performance of these bimetallic electrocatalysts in comparison to Pt is due to their bi-functional mechanism and/or the ligand/electronic effects [28–31]. Several studies have revealed that the incorporation of oxophilic metals such as Sn and Ru, and Mo, can enhance the dissociative adsorption of water to form the surface hydroxides species at lower electrode potentials during electrooxidation of ethanol molecule. These surface hydroxides species can promote the oxidation of poisoning substances like CO and CH_x intermediates on adjacent active sites and thereby assisting in regeneration of active sites for further oxidation via bifunctional mechanism [10,28,29]. The ligand or electronic effects are also thought to play an important role over enhanced electrocatalytic activity of Pt-Ru bimetallic alloy electrocatalysts, which is based on the weakening the bond strength of Pt-CO by modification of Pt electronic structure with the presence of Ru surface atoms that enhances CO oxidation to CO_2 [30,31].

It is seen from the literature that the activity of the electrocatalysts for splitting ethanol molecules strongly depends on particle size, particle size distribution, as well as dispersion of electrocatalyst nanoparticles on the surface of support material, employed [29]. The support materials also play an important role by lowering the use of noble metal particles and simultaneously improving the electrocatalytic activity by providing large surface area for better dispersion, high electrical conductivity and porous structure for better diffusion of reactants to reaction sites [1,32]. The highly conducting carbon blacks with high surface area along with its graphitic characteristic are most commonly used electrocatalyst support material in low temperature fuel cells. Among all carbon support materials, Vulcan XC-72 is widely used support material by considering its physical properties. However, Vulcan XC-72 contains a large number of micropores of less than 1 nm (30% of S_{BET} area) which resists the reactant accessibility [33,34]. Thus, an important portion of electrocatalyst nanoparticles could be sunk into the micropores and remain unutilized. Moreover, Vulcan XC-72 is very expensive and not available easily.

In the last few decades, growing literature has appeared concerning novel non-conventional carbon supports materials like carbon nanotubes (CNTs) [4,19]. Carbon nanotubes (CNTs) offer outstanding properties like excellent electrical conductivity and high chemical stability but they have poor pore development and low surface area compared to carbon black Vulcan XC-72(R). CNTs are two-dimensional tubular nanostructures, which consists of single sheets of hexagonally arranged carbon networks i.e., graphene and generally categorized as single-walled carbon nanotubes (SWNTs) or multi-walled carbon nanotubes (MWCNT). The SWNTs contain larger surface area, while MWCNTs having higher electrical conductivity [4,19,32]. However, the preparation cost of novel non-conventional carbon support likes CNTs is higher than conventional carbon support, which limit its availability at low cost. For these reasons, carbon support materials like acetylene black which is cheaper, easily available and highly dispersed nanostructured could be treated as suitable support material for synthesis of bimetallic electrocatalyst for ethanol electrooxidation.

The pretreatment of carbon support via HNO_3 functionalization and the preparation procedure of electrocatalyst synthesis have a great influence on the particle size and dispersion of metal particle over the support surface. The carbon-supported electrocatalysts are generally synthesized by the impregnation, the colloidal and the microemulsion methods [35,36].

The oxidation of carbon support materials has been reported to influence the electrochemical activities of the electrocatalysts for the ethanol electrooxidation [37–39]. The chemical functionalization treatment of carbon support via oxidizing solutions of HNO_3, HNO_3–H_2SO_4 or H_2O_2 results in formation of different oxygen functionalities on carbon surfaces, such as carboxyls, carbonyls, phenols, quinones or lactones [37,38,40]. These oxygenated species has been reported to be beneficial for getting a better metal dispersion and anchoring of the electrocatalytic active phase onto the carbon surface. Furthermore, oxygenated surface species also enhance the hydrophilic character of carbons and favoring the diffusion of the reactants to the active sites [40,41].

The polyol reduction process is one of the most powerful technique in which a polyol such as ethylene glycol used as both a solvent and reductant of metallic precursors along with controlling the pH of the solvent with NaOH. Recently, polyol reduction method has received great attention as it provides accurate size control and well dispersed metal nanoparticles over support material without needing any additional stabilizers. In the polyol reduction process, Pt-Ru metal colloids are stabilized by glycolate produced from ethylene glycol oxidation in alkaline medium [42,43]. Lee et al. [44] evaluated the performance of post treated polyol synthesized bimetallic Pt-Ru/C electrocatalysts for methanol electrooxidation. Post treated Pt-Ru/C at room temperature in H_2 atmosphere exhibited higher intrinsic activity in half and single cell test performance due to lower phase separation and agglomeration of particles.

Zhiani et al. [45] studied methanol electrooxidation in acidic media on Pt-Ru/acetylene black (20:10 wt %) electrocatalyst synthesized by direct reduction of precursor solution containing acetylene black by $Na_2S_2O_4$. It was observed that the electrocatalytic activity of synthesized Pt-Ru/acetylene black (20:10 wt %) electrocatalyst was higher than the commercial Pt-Ru/C (20:10 wt %) in both half-cell and single direct methanol fuel cell experiments. Recently, we reported the effect of synthesis methods on the electrocatalytic activities of bi-metallic Pt-Ru nano electrocatalysts supported on functionalized acetylene black as anode electrocatalysts for ethanol electrooxidation in acidic media [46]. The performance of synthesized electrocatalysts for ethanol electrooxidation in acidic media was superior to the commercial Pt-Ru/C (30:15 wt %).

Although, many researchers [37–40] have studied the pretreatment of support material for the synthesis of bi-metallic electrocatalysts to split ethanol molecule electrochemically almost no such paper was found on post treatment of functionalized acetylene black (C_{AB}) supported Pt-Ru electrocatalyst for ethanol electrooxidation at moderate temperature.

In this context, the influence of post-treatment in reduction and oxidation atmospheres along with temperature effects on the modified polyol synthesized electrocatalysts were investigated. The promoted surface structures, morphology, alloying degree and elemental composition of the electrocatalysts were analyzed by X-ray diffraction (XRD), scanning electron microscopy (SEM), transmission electron microscopy (TEM), and energy dispersive X-ray (EDX) analysis. The electrochemical activity for ethanol dissociation and stability of the synthesized electrocatalysts were investigated and compared with the commercial Pt-Ru/C using cyclic voltammetry (CV) and chronoamperometry (CA) measurement tests at a temperature of 40 °C. Finally, the synthesized electrocatalysts were tested as anode in single-cell DEFCs experiment tests to verify the cell performance in terms of open circuit voltage (OCV) and cell power densities.

Experimental method

Materials

Chloroplatinic (IV) acid hexahydrate (20 wt % Pt, $H_2PtCl_6.6H_2O$) and ruthenium (III) chloride (48.2 wt %, $RuCl_3$) were purchased from Alfa Aesar (USA) and used as metal precursors for the synthesis of electrocatalysts. The commercial Pt-Ru/C (30%:15% by wt., Alfa Aesar) was used as anode electrocatalyst to compare the electrocatalytic activity with the synthesized electrocatalysts. The carbon support acetylene black (S_{BET} = 75 m^2/g and average particle size of 40–60 nm) was procured from Alfa Aesar, USA. Nafion® (D-520, 5 wt %) dispersion and commercial Nafion® 117 membrane/solid electrolyte were bought from Alfa Aesar, USA. Ethylene glycol (≥99.0%), isopropanol (99.5%), $HClO_4$ (70%), and HNO_3 (69–71%) were manufactured by Fisher Scientific, India. Ethanol (99.9%, Merck, Germany) was used as fuel. The polytetrafluoroethylene (PTFE) dispersion (60 wt %, Sigma-Aldrich, Germany) was used as for electrode manufacturing. Toray carbon paper (TGP-H-60, Alfa Aesar, USA) was used as a substrate or gas diffusion layer (GDL) to paint electrocatalyst ink of electrode. The commercial Pt (40 % wt.)/High surface area carbon black (C_{HSA}) (Alfa Aesar, USA) was employed as cathode electrocatalyst.

Functionalization of electrocatalyst support material

First of all, the support material pristine acetylene black (C_{PAB}) carbon powder was washed with distilled water to reduce its initial organic impurities present. The oxygenated functional groups were introduced over the surface of carbon support by mixing with the calculated amount of pristine acetylene black powder in 65 wt % HNO_3 using an ultrasonic water bath at a temperature of 35 °C for 30 min. The suspended mixture was then refluxed at a temperature of 140 °C for 6 h under vigorous stirring [34,47]. Finally, the mixture suspension was diluted with distilled water, filtered and rinsed with distilled water until the pH is neutral. The obtained residue was then dried at a temperature of 80 °C for 12 h. The resulting functionalized/treated acetylene black carbon (C_{AB}) was used as support material for synthesis of bi-metallic Pt-Ru supported electrocatalysts via several post treatment route which are discussed in the section below.

Electrocatalyst preparation

The modified polyol reduction route as adopted by Wang et al. [43], Lee et al. [44], and Lee et al. [48] were used for the synthesis of carbon supported Pt-Ru (Pt: Ru atomic ratio = 1:1) nano electrocatalysts with nominal metal loading of 40 wt % on carbon support C_{AB} of 60 wt %. The calculated amount of metal precursors $H_2PtCl_6.6H_2O$ and $RuCl_3$ were dissolved in aqueous ethylene glycol solution (Distilled water 5% by volume) and subjected to ultrasonic dispersion for 3 h. The pH of the above suspension was being adjusted to 12–13 approximately by addition of 1 M NaOH solution in ethylene glycol drop wise and kept under stirring for 30 min in air at room temperature of 30 °C. Subsequently, the suspension mixture was transferred to a three necked flask and refluxed at a temperature of 140 °C for 4 h to obtain dark brown PtRu colloidal nanoparticles. The reaction system was purged with the high purity nitrogen gas to expel out the dissolved oxygen and organic byproducts. A requisite amount of functionalized/treated carbon support was dispersed separately in aqueous ethylene glycol solution (ethylene glycol: distilled H_2O = 1:1 by volume) by ultrasonic treatment for 3 h and stirred vigorously for 1 h for homogeneously mixing. The as synthesized Pt-Ru colloidal nanoparticles were mixed with carbon dispersed suspension by sonication, and again the pH was adjusted to about 2 using a few drops of 2 M H_2SO_4 solution. The resulted suspension mixture was heated at a temperature of 80 C° and maintained at that temperature for 6 h under vigorous stirring to deposit Pt-Ru colloidal nanoparticles on the carbon support surface. Finally, the black suspension was cooled to room temperature and filtered followed by washing extensively with distilled water. The filtered cleaned precipitate was dried in a vacuum oven at a temperature of 80 °C for 12 h and homogeneously ground to fine powder using a mortar and pestle. The obtained electrocatalyst power was denoted as Pt-

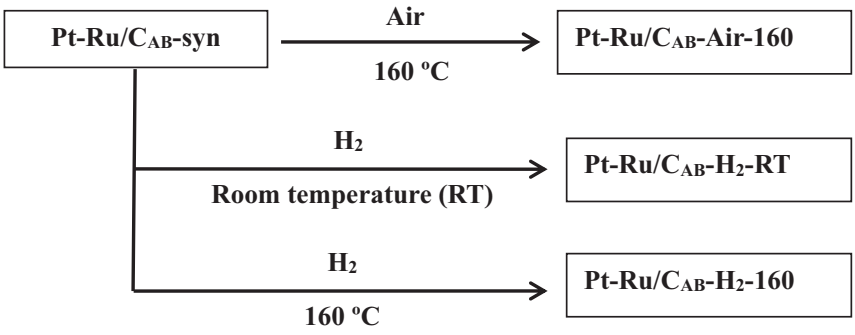

Fig. 1 – Scheme of post-treated conditions of the Pt-Ru/C$_{AB}$-syn electrocatalyst by modified polyol method.

Ru/C$_{AB}$-syn. The Pt-Ru/C$_{AB}$-syn electrocatalyst were post treated in a tube furnace under three different conditions (i) in high purity hydrogen gas at room temperature (30 °C) for 1 h, (ii) with high purity hydrogen gas at 160 °C for 1 h and (iii) under air at 160 °C for 1 h (Fig. 1). The synthesized electrocatalysts were designated as Pt-Ru/C$_{AB}$-H$_2$-RT, Pt-Ru/C$_{AB}$-H$_2$-160, and Pt-Ru/C$_{AB}$-Air-160 as per above defined conditions (i), (ii) and (iii), respectively.

Reaction mechanism of modified polyol reduction process

There are several reaction mechanisms for the modified polyol reduction have already discussed many in previous studies [42,51–53]. In modified polyol reduction method, Pt and Ru are co-reduced and deposited on substrates surface from their ionic salts dissolved in ethylene glycol-water solution. In the first step of the modified polyol method, at high pH (≥12) metal hydroxide colloid is formed by the hydrolysis reaction between metal salt ions and NaOH via following reaction (Eq. (6)) as proposed by Wang et al. [54].

$$PtCl_6^{2-}\ or\ Ru^{3+} + OH^- \Big/ NaOH \xrightarrow{Ethykene\ glycol-water\ (pH\geq 12)} Pt(OH)_X\ or\ Ru(OH)_Y \quad (6)$$

Further, the generated metal hydroxide colloids were reduced after receiving the electrons from the oxidation of ethylene glycol to glycolic acid as per the reaction mechanism proposed by Bock et al. [42]. Since, ethylene glycol is a very weak acid which can be thermally (140 °C) oxidized to aldehydes by the interaction of OH^- groups of ethylene glycol with Pt and Ru ions sites.

$$CH_2OH{-}CH_2OH \rightarrow CH_2OH{-}CHO + 2H^+ \rightarrow HCO{-}CHO + 2H^+ \quad (7a)$$

$$CH_2OH{-}CHO \rightarrow CH_2OH{-}COOH \quad (7b)$$

$$CH_2OH{-}COOH \text{ or } HCO{-}CHO \rightarrow COOH{-}COOH \quad (7c)$$

$$COOH{-}COOH \rightarrow 2CO_2 + 2H^+ \text{ or carbonate} \quad (7d)$$

The unstable aldehydes formed in the reaction mechanism (Eq. (7a)) are not very stable and undergo further oxidation to form glycolic acid (Eq. (7b)) and oxalic acid (Eq. (7c)), respectively. These two carboxylic acids may further be oxidized to CO_2 or carbonate (Eq. (7d)) in alkaline media. The electrons donated by oxidation reactions result in the reduction of the Pt and Ru metal ions to form Pt-Ru metal colloids via Eq. (8).

$$xPt^{4+} + xRu^{3+} + \frac{7}{2}x\,H_2\,(HO)\,CC\,(OH)\,H_2 \xrightarrow{NaoH/\Delta T} (Pt_x/Ru_x) - colloids + \frac{7}{4}x\,(HO)OCC\,(OH)H + \frac{7}{2}x\,H^+ \quad (8)$$

In alkaline medium, glycolic acid is present in the form of glycolate anion (deprotonated state) act as a stabilizer by forming chelate-type complexes via its carboxyl groups [42,55]. The stabilizing effect of glycolate anion concentration is a function of pH of the reaction mixture. The glycolate anion concentration is expected to remain constant at higher pH (pH ≥ 6). The stabilizing effect of glycolate anion helps in controlling the particle size of Pt-Ru metal colloids. However, the stabilizing effect of glycolate anion destroyed due to higher concentrations of protons and Cl^- ions when pH value is reduced to about 2. The glycolate anion is replaced by glycolic acid (protonated state) which is a poor stabilizer and, consequently reduced Pt-Ru metal particles are deposited on the carbon support active sites.

Physical characterization of the electrocatalysts

The structural characteristics of the synthesized electrocatalysts were investigated by means of a XRD (Rigaku Ultima IV, Germany) using Cu Kα radiation source (λ = 0.154056 nm) with a Ni filter, operating at 40 kV and 15 mA. The samples were explored the 2θ scanning angle from 10° to 90° with a 0.02° step size at a scan rate of 5° min^{-1}.

The particle size and dispersion morphology Pt-Ru nanoparticles were evaluated using a TEM (Tecnai G2 20 Twin, FEI

Company, USA) operated at 200 kV. Prior to the measurement, the specimens for TEM analysis were prepared by applying a single drop of ultrasonically dispersed suspension of each electrocatalyst by a micropipette on the carbon coated Cu grid of 200 mesh size, followed by drying at a temperature of 60 °C in a vacuum oven for 3 h. The particle size distribution histogram was obtained by measuring sizes of 150 metal nanoparticles from each TEM image using Image J software.

The surface structure and morphologies of dispersed electrocatalysts were investigated by SEM-EDX (Nova Nano SEM 450, FEI Company U.S.A). The chemical composition of existing elements of the electrocatalyst was evaluated by EDX analyzer using Octane Plus SDD detector attached to a SEM instrument.

Electrochemical studies of electrode

All the electrochemical measurments of the anode electrocatalysts were accomplished at a temperature of 40 °C using potentiostat/Galvanostat (Autolab Model PGSTAT 204, Netherland) in a conventional three-electrode assembly test cell. A silver chloride electrode (Ag/AgCl in saturated KCl) and a long platinum wire were employed as the reference and the counter electrodes, respectively. The carbon paper coated with Nafion®-impregnated electrocatalyst ink was used as the working electrode. To manufacture the working electrode, the electrocatalyst ink (100 μL) was prepared by mixing 2 mg electrocatalyst powder in 5 μL Nafion® (5 wt %) solution and the appropriate amount of isopropanol under ultrasonic treatment in a water bath at a temperature of 35 °C for 30 min. The prepared electrocatalyst ink was deposited on the tip of 0.25 cm^2 area of a long strip of carbon paper, followed by drying at a temperature of 80 °C for 1 h. Prior to the electrochemical measurements, high purity nitrogen gas was bubbled through the electrolyte and fuel solution (0.5 M $HClO_4$ + 2 M C_2H_5OH) at a flow rate of 10 mL/min using silicon tubing for 30 min to remove dissolve oxygen.

Membrane electrode assembly (MEA) fabrication and single-cell DEFC test

The electrocatalysts tested in the anode side were synthesized electrocatalysts Pt-Ru/C_{AB}-H_2-RT, Pt-Ru/C_{AB}-H_2-160, Pt-Ru/C_{AB}-Air-160 and commercial Pt-Ru/C, respectively. The anode loading in all cases were same in the range of 1 mg/cm^2. The commercial Pt/C_{HSA} electrocatalyst was used at cathode side of 1 mg/cm^2 in all experiments. The electrocatalyst ink/slurry was prepared by dipersing the required amount of electrocatalyst powder, Nafion® ionomer solution (30 wt % of solid content of the slurry), isopropanol and a few drops of PTFE dispersion using an ultrasonic water bath at a temperature of 35 °C for 30 min. The prepared electrocatalyst ink/slurry was then uniformly spread on the porous gas diffusion layer/GDL using a thin brush. Subsequently, the composite structure of the electrodes was dried in an oven at a temperature of 80 °C for 1 h to evaporate the solvent. Finally, the dried anode and cathode electrodes were sintered in a vacuum oven at a temperature of 300 °C for 3 h, to get the porous structure of the anode and cathode, respectively. It should be noted that the fabrication procedure of anode and cathode were similar expect the electrocatalyst used. The active surface area of the anode and cathode electrodes was 6.25 cm^2 (2.5 cm × 2.5 cm). Finally, the MEA was made by keeping the commercial Nafion® 117 membrane in between the sintered anode and cathode electrodes followed by clamping the assembly together without hot pressing [49,50].

The performances of synthesized electrocatalysts as anode in single cell-DEFCs were evaluated using a commercial fuel cell set-up (Fig. 2a). The fabricated MEA was inserted in between two serpentine graphite flow channel plates which were attached by two gold plated copper current collectors from outside of the flow channel plates. The cell was then fixed by bolts tightening at the four corner of the cell assembly end plate with a uniform torque. The DEFC tests were conducted with constant supply of fuel (2 M) ethanol at a flow rate of 1.2 ml/min to the anode side using a peristaltic pump (Electrolab, India) and 60 ml/min of humidified oxygen gas to the cathode side from an oxygen cylinder. The fuel cell tests were conducted at a moderate temperature range of 40 °C–80 °C and 1 bar (absolute) pressures both sides of the electrodes.

The pictorial view of the experiment set-up assembly is also depicted in Fig. 2b. The polarization curves, V-I data were recorded by measuring the cell voltage at different currents using DC Electronic Load Bank (K-PAS, India) after reaching the cell performance steady state for each set of experiments.

Results and discussion

Structural and morphological characterization of electrocatalysts

X diffraction (XRD) analysis

The XRD measurements were obtained to investigate the crystal characteristics of electrocatalysts and results are presented in Fig. 3. The first broad diffraction peak at around $2\theta = 25.3°$ is associated with the carbon/graphite (002) crystalline plane of its hexagonal structure for all the samples.

The Pt-Ru/C_{AB}-syn fresh electrocatalyst display a broad diffraction peak at 38.7° which is due to superposed effect of RuO_2 at 35.2° (101) and Pt diffraction peak at 39.7° (111), while the other diffraction peaks at Pt (200), Pt (220), Pt (311) and Pt (222) are too weak to be observed. The XRD pattern of Pt-Ru/C_{AB}-syn electrocatalyst reveals its poor crystalline structure. After the post treatment in a reductive (H_2) atmosphere, the RuO_2 peaks disappear from the post treated Pt-Ru/C_{AB}-H_2-RT and Ru/C_{AB}-H_2-160 electrocatalysts. However, post treated in an oxidative (air) atmosphere increased the crystallinity of Pt-Ru/C_{AB}-Air-160 electrocatalyst. The three additional peaks at 28.1°, 35.2° and 54.4° were observed for Pt-Ru/C_{AB}-Air-160 electrocatalyst can be indexed to the (110), (101) and (211) planes of anhydrous crystalline rutile RuO_2 (JCPDS no. 43-1027). This suggests that the RuO_2 and Pt phase are separated further during post treatment under oxidative atmosphere. The lack of characteristic diffraction peaks of metallic Ru or Ru oxides/hydroxides in the XRD patterns of the post treated under reductive atmosphere and commercial electrocatalysts, suggests that Ru atoms form metal alloy with Pt atoms or exist as oxides in amorphous form [56,57]. On the other side, the

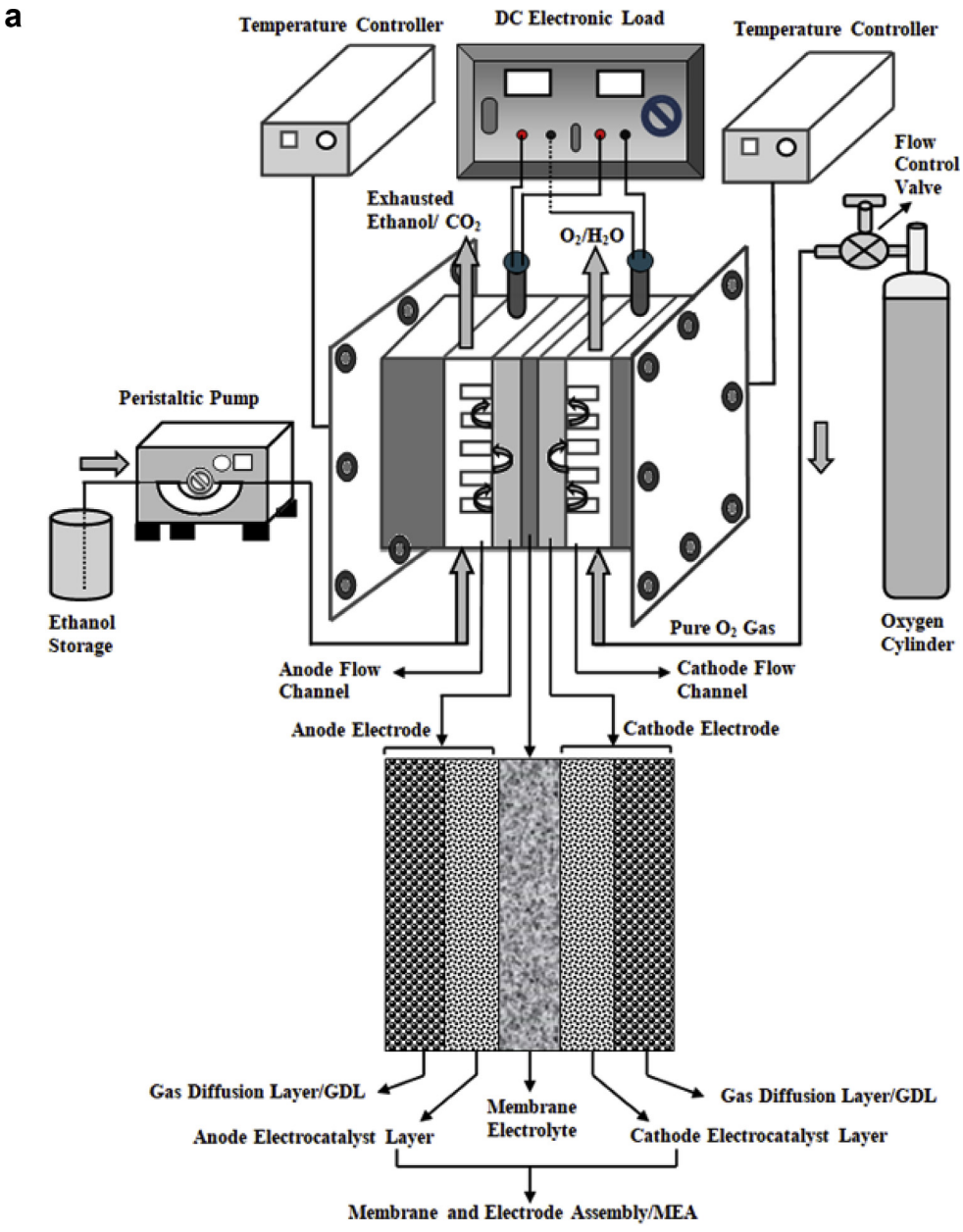

Fig. 2 – a. Schematic diagram of single-cell direct ethanol fuel cell set up. b The pictorial view of the single cell test assembly.

XRD patterns of Pt-Ru/C_{AB}-H_2-RT, Pt-Ru/C_{AB}-Air-160, Pt-Ru/C_{AB}-H_2-160 and commercial Pt-Ru/C electrocatalysts represent the typical face-centered cubic (FCC) crystalline Pt diffraction peaks. The XRD patterns of all the Pt-Ru/C electrocatalysts samples except Pt-Ru/C_{AB}-sny showed the Pt diffraction peaks shifting to higher 2θ degree compare to pure Pt diffraction peaks, which reveals that the Ru atoms (smaller than Pt) are incorporated into Pt crystal lattice to form a FCC solid solution between Pt and Ru. The Pt (220) peak was selected to estimate the average crystallite size (d_c) of electrocatalysts samples based on the Debye Scherrer equation [43]. The Pt (220) peak was chosen due to its relative isolation from carbon contributions. The average crystallite size of the Pt-Ru/C_{AB}-syn electrocatalyst could not be calculated due to weak intensity of Pt (220) diffraction peak.

The Ru atomic fraction (x_{Ru}) in the bimetallic Pt-Ru/C electrocatalysts were measured using Vegard's law [58], which is based on the shifting of Pt diffraction peaks and variation in lattice parameters from the XRD patterns. Antolini and Cardelline [59] proposed a linear relationship between the lattice parameter and the alloyed Ru atomic fraction (<0•7) as mentioned below:

$$a_{(Pt-Ru/c)} = a_{(Pt/c)} - kx_{Ru} \quad (9)$$

Here, x_{Ru} describes Ru atomic fraction in PtRu alloy, and $a_{(Pt/C)}$ and $a_{(Pt-Ru/C)}$ are the lattice parameter of Pt/C and the Pt–Ru/C alloyed electrocatalyst, respectively. The value of constant k (0.0124 nm) and the lattice parameter of Pt/C ($a_{(Pt/C)}$=0.3916 nm) were taken from literature data [60]. The values of x_{Ru} calculated via Eq. (9) of all the bimetallic electrocatalysts are reported in Table 1. The resulting average crystallite size, lattice parameters and alloying degree related to Pt (220) peak of the electrocatalysts from the XRD patterns are listed in Table 1.

The alloying degree of Ru (Ru_{alloy}) in the bimetallic supported Pt-Ru electrocatalysts was calculated using the following relationship (Eq. (10)):

$$Ru_{alloy} = \frac{x_{Ru}}{\left[(1 - x_{Ru})\left(\frac{Ru}{Pt}\right)_{nom}\right]} \quad (10)$$

Here, $\left(\frac{Ru}{Pt}\right)_{nom}$ represents the nominal atomic ratio of Ru to Pt and x_{Ru} is the atomic content of alloyed Ru fraction in the Pt-Ru/C alloy electrocatalysts.

The average crystallite sizes for Pt (220) of the Pt-Ru/C_{AB}-H_2-RT, Pt-Ru/C_{AB}-Air-160, Pt-Ru/C_{AB}-H_2-160 and commercial Pt-Ru/C electrocatalysts were calculated to be 3.2 nm, 3.5 nm, 3.8 nm, and 2.8 nm, respectively. It is also observed that the lattice parameters of the Pt-Ru/C_{AB} electrocatalysts are in the range of 0.3877 0.3899 nm, which is lower than that of pure Pt (0.3923 nm) or Pt/C (a = 0.3916 nm) [60,61]. The alloying degree of the Pt-Ru/C_{AB}-H_2-RT electrocatalyst was as high as 40.84%. Whereas, fresh synthesized electrocatalyst Pt-Ru/C_{AB}-syn showed Ru alloying of 2.49% only. This indicates that most of the RuO_2 in the as synthesized Pt-Ru/C_{AB}-syn electrocatalyst is further reduced by the H_2 flow at room temperature and improves its alloy formation. When the post treatment reduction temperature was increased to 160 °C in the presence of H_2 flow, caused drastic agglomeration of crystallite size and alloying degree of Ru/C_{AB}-H_2-160 was lower (27.71%) than that of post treated electrocatalyst at room temperature/Pt-Ru/C_{AB}-H_2-RT (40.84%). The post treated electrocatalyst in the presence of air at a temperature of 160 °C (Pt-Ru/C_{AB}-Air-160) showed the lowest alloying degree of about 15.87% due to lack of reducing environment. It is clearly observed in Table 1 that the amount of Ru alloyed with Pt is smaller than nominal values, which suggest that a part of Ru is present as oxides in the amorphous form on the electrocatalyst surface and cannot be detected by XRD measurements [28,57].

SEM and EDX analysis

The SEM images and corresponding EDX patterns of the synthesized and commercial bimetallic electrocatalysts are presented in Fig. 4a–e. The elemental compositions and metal loading on the carbon support of the electrocatalysts are examined by EDX spectrum.

It is clearly seen in Fig. 4a–e that the electrocatalysts particles are of nano-range and their surface morphology is uniform. The SEM images also confirm that the synthesized electrocatalysts are made of porous spherical particles which could facilitate mass transport from the bulk phase to the active electrocatalysts sites. The EDX spectrum of all the electrocatalysts reveals the presence of desired elements such as Pt, Ru, and C respectively; which can be ascribed to the Pt-Ru electrocatalyst nanoparticles supported on the carbon support. The strongest C peaks in all EDX patterns were observed due to the presence of the acetylene black support material. Post treatment does not promote significant alterations in the EDX nominal values. The average elemental compositions of all the electrocatalysts evaluated by EDX analyses are summarized in Table 2. Total metal loading on the carbon support was around 40 wt % and was similar in each case. The desired elements compositions were nearly in good agreement with the nominal compositions with some variations.

The presence of common impurity such as chlorine was also observed. However, traces of chlorine impurity is almost negligible and may be attributed due to the remains of metal precursors used in electrocatalyst synthesis. The presence of oxygen indicates the formation of ruthenium oxides or

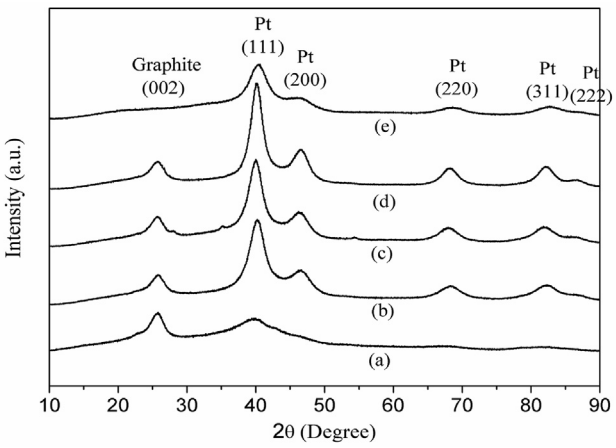

Fig. 3 – XRD patterns of (a) Pt-Ru/C_{AB}-syn, (b) Pt-Ru/C_{AB}-H_2-RT, (c) Pt-Ru/C_{AB}-Air-160, (d) Ru/C_{AB}-H_2-160 and (e) commercial Pt-Ru/C electrocatalysts.

Table 1 – Data obtained from XRD patterns analyses by Debye Scherrer formula and Vegard's law.

Electrocatalysts	Average crystallite size (d_c) (nm)	Lattice parameter (a) (nm)	Pt (2 2 0) peak position 2θ (°)	Ru fraction (x_{Ru})	Alloyed Ru (wt.%)
Pt-Ru/C_{AB}-syn	–	0.3913	67.63	0.024	2.49
Pt-Ru/C_{AB}-H_2-RT	3.2	0.3880	68.30	0.290	40.84
Pt-Ru/C_{AB}-Air-160	3.5	0.3899	67.90	0.137	15.87
Pt-Ru/C_{AB}-H_2-160	3.8	0.3889	68.11	0.217	27.71
Commercial Pt-Ru/C	2.8	0.3877	68.35	0.315	45.98

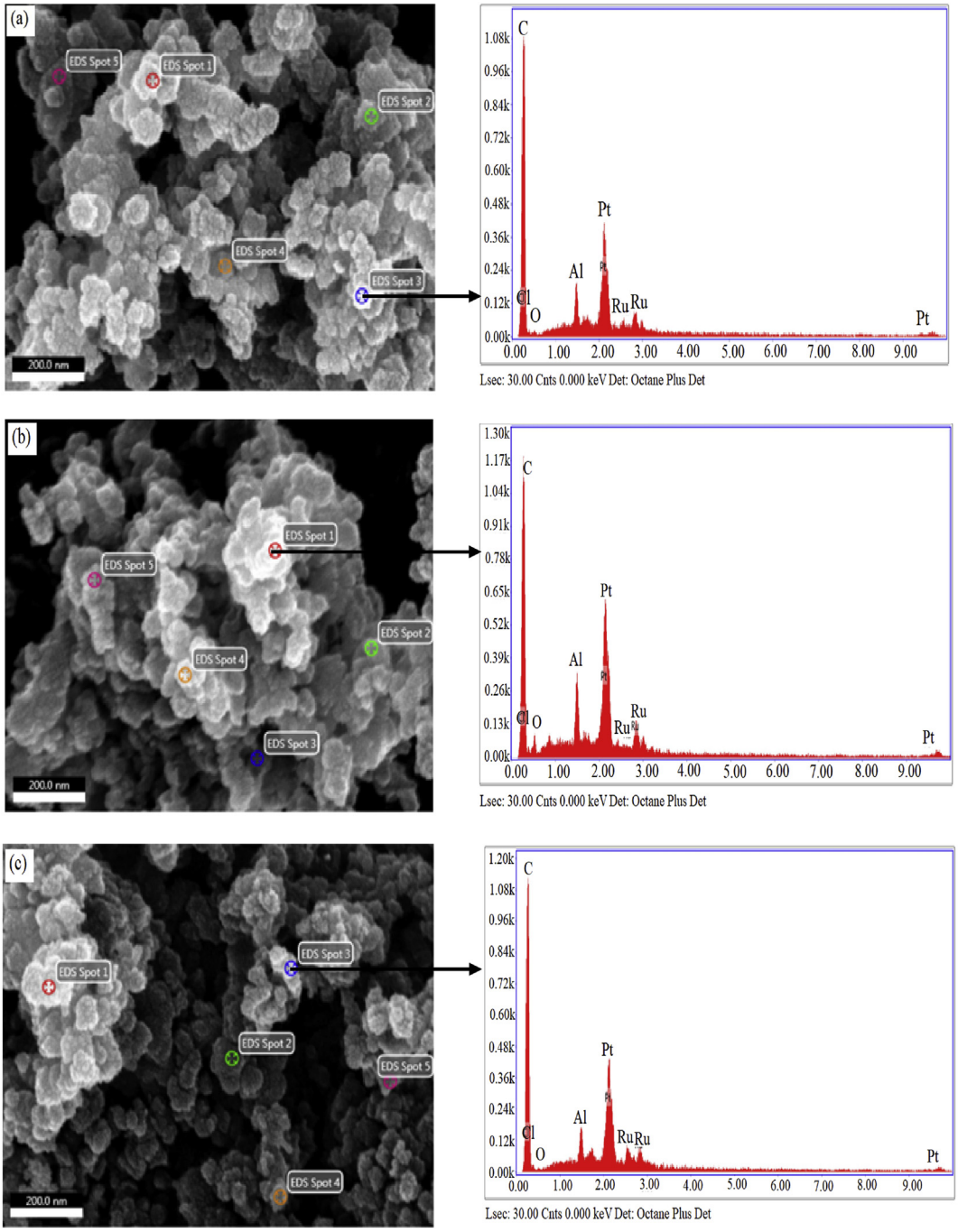

Fig. 4 – SEM images and corresponding EDX patterns of (a) Pt-Ru/C_{AB}-syn, (b) Pt-Ru/C_{AB}-H_2-RT, (c) Pt-Ru/C_{AB}-Air-160, (d) Ru/C_{AB}-H_2-160, and (e) commercial Pt-Ru/C electrocatalysts.

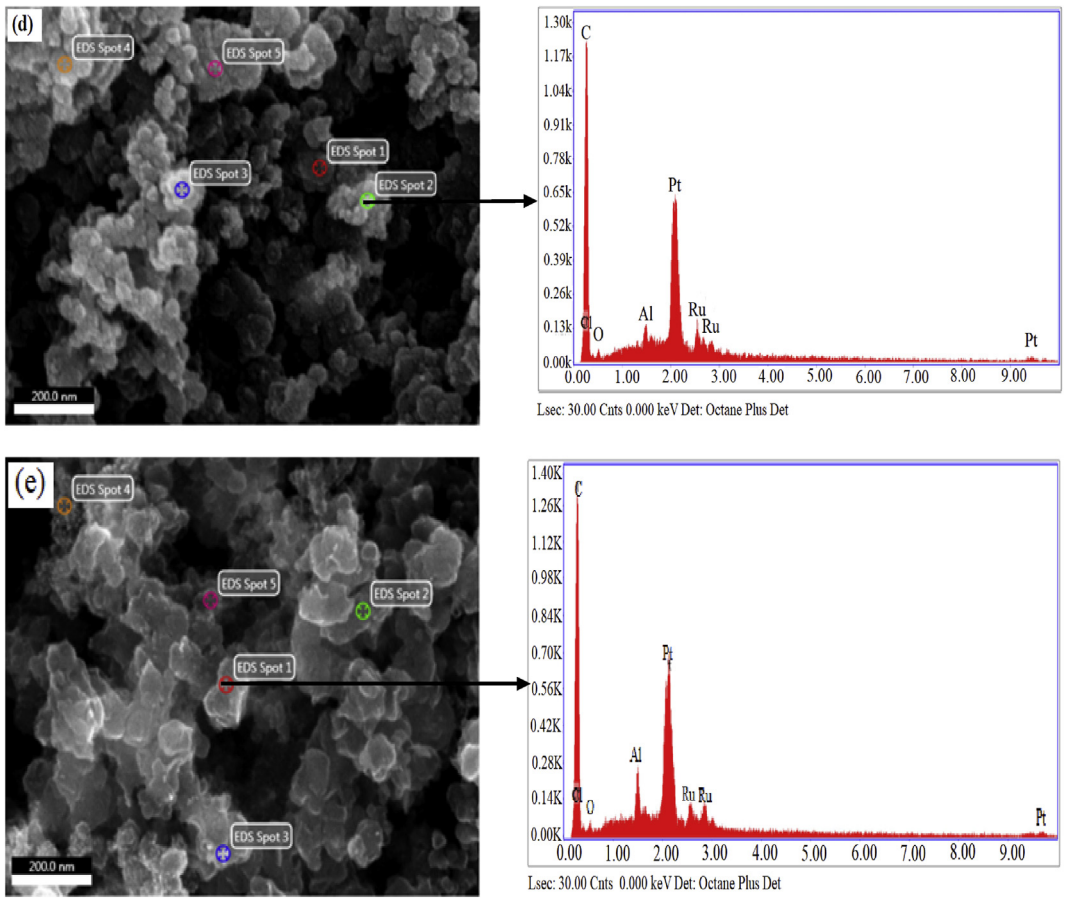

Fig. 4 – *(continued)*.

platinum oxides which have been reported by many other investigators for Pt-Ru/C electrocatalysts [28,62]. The presence of chlorine common impurity has also been reported by Tayal et al. [23]. The peak of aluminum at 1.5 eV was also observed during EDX analysis, which originates from sample holder [23,63].

TEM analysis

The dispersed state, particle size and particle size distribution histogram of the electrocatalysts were analyzed by TEM (Fig. 5a–e). It is seen in Fig. 5a–e, most of the nanoparticles are homogeneously distributed on the carbon support surface in all the electrocatalysts. The histogram of the particle size distribution reflects the size distribution in the Pt-Ru/C_{AB} electrocatalysts quantitatively. The heavy dark spots represent Pt-Ru metal alloy nanoparticles, which are well dispersed over the lighter particles carbon support surface (40–60 nm size). The electrocatalysts synthesized by modified Polyol method show well dispersed metal nanoparticles on the carbon support with varying degree of dispersion. Fig. 5a shows that synthesized fresh Pt-Ru/C_{AB}-syn electrocatalyst nanoparticles are not contacted each other due to the adsorption of glycolate acid on metal nanoparticles and carbon support which preventing the interconnection of nanoparticles.

However, when the Pt-Ru/C_{AB}-syn electrocatalyst undergoes post treatment in H_2 gas stream at room temperature (30 °C), the nanoparticles interconnected together to form bigger particles. This indicates that the post treatment of electrocatalyst in H_2 gas flow modifies the morphological

Table 2 – EDX compositions of synthesized Pt–Ru/C_{AB}-syn, Pt–Ru/C_{AB}-H_2-RT, Pt–Ru/C_{AB}-Air-160, and Pt–Ru/C_{AB}-H_2-160 electrocatalysts.

Electrocatalysts	Nominal Composition (wt. %)	Composition obtained by EDX (wt. %)	Composition obtained by EDX (at. %)
Pt-Ru/C_{AB}-syn	Pt: 26.35, Ru:13.65, C: 60	Pt: 25.71, Ru: 12.93, O: 1.16, C: 60.2	Pt: 50.75,Ru: 49.25
Pt-Ru/C_{AB}-H_2-RT	Pt: 26.35, Ru:13.65, C: 60	Pt: 24.62, Ru: 12.59, O: 3.59, C: 59.20	Pt: 50.33,Ru: 49.67
Pt-Ru/C_{AB}-Air-160	Pt: 26.35, Ru:13.65, C: 60	Pt: 25.40, Ru: 12.51, O: 2.80, C: 59.29	Pt: 51.27,Ru: 48.73
Pt-Ru/C_{AB}-H_2-160	Pt: 26.35, Ru:13.65, C: 60	Pt: 25.81, Ru: 12.10, O: 1.80, C: 59.39	Pt: 52.50,Ru: 47.50
commercial Pt-Ru/C	Pt: 30, Ru:15, C: 55	Pt: 28.40, Ru: 13.28, O: 1.77, C: 56.55	Pt: 52.56,Ru: 47.44

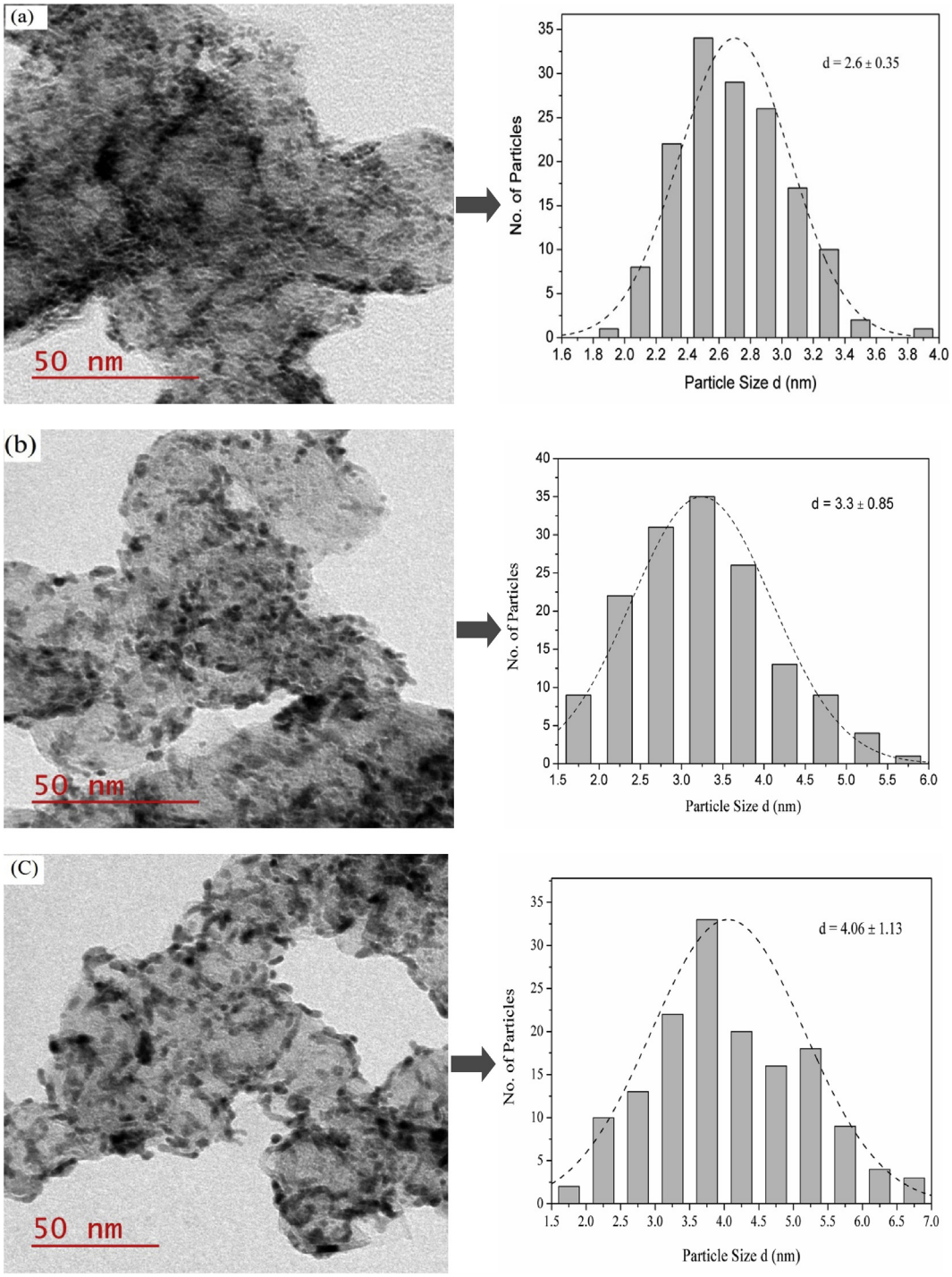

Fig. 5 – TEM images and corresponding size distribution histograms of (a) Pt-Ru/C_{AB}-syn, (b) Pt-Ru/C_{AB}-H_2-RT, (c) Pt-Ru/C_{AB}-Air-160, (d) Ru/C_{AB}-H_2-160 and (e) commercial Pt-Ru/C electrocatalysts.

structures of the Pt-Ru/C_{AB}-H_2-RT electrocatalyst and crystallite size. Post treatment in an air stream at a temperature of 160 °C also modified slightly morphological structures and growth of nanoparticles is also observed in the Pt-Ru/C_{AB}-Air-160 electrocatalyst. When the electrocatalyst was post treated under H_2 gas flow stream at a temperature of 160 °C, greatly promoted further agglomeration and interconnection of metal nanoparticles as observed in the Pt-Ru/C_{AB}-H_2-160 electrocatalyst (Fig. 5d). The particle size for Pt-Ru/C_{AB}-syn electrocatalyst ranges from 1.5 to 4 nm, with an average particle size of 2.6 ± 0.35 nm. The average particle size for Pt-Ru/C_{AB}-H_2-RT synthesized electrocatalyst is 3.3 ± 0.85 nm and the size distribution lie in the range of 1.5–6 nm. Similarly, for the commercial Pt-Ru/C electrocatalyst, the average particle size is 3.0 ± 0.58 nm and size distribution ranges from 1.5 to 5.5 nm, which is very close to the synthesized post treated

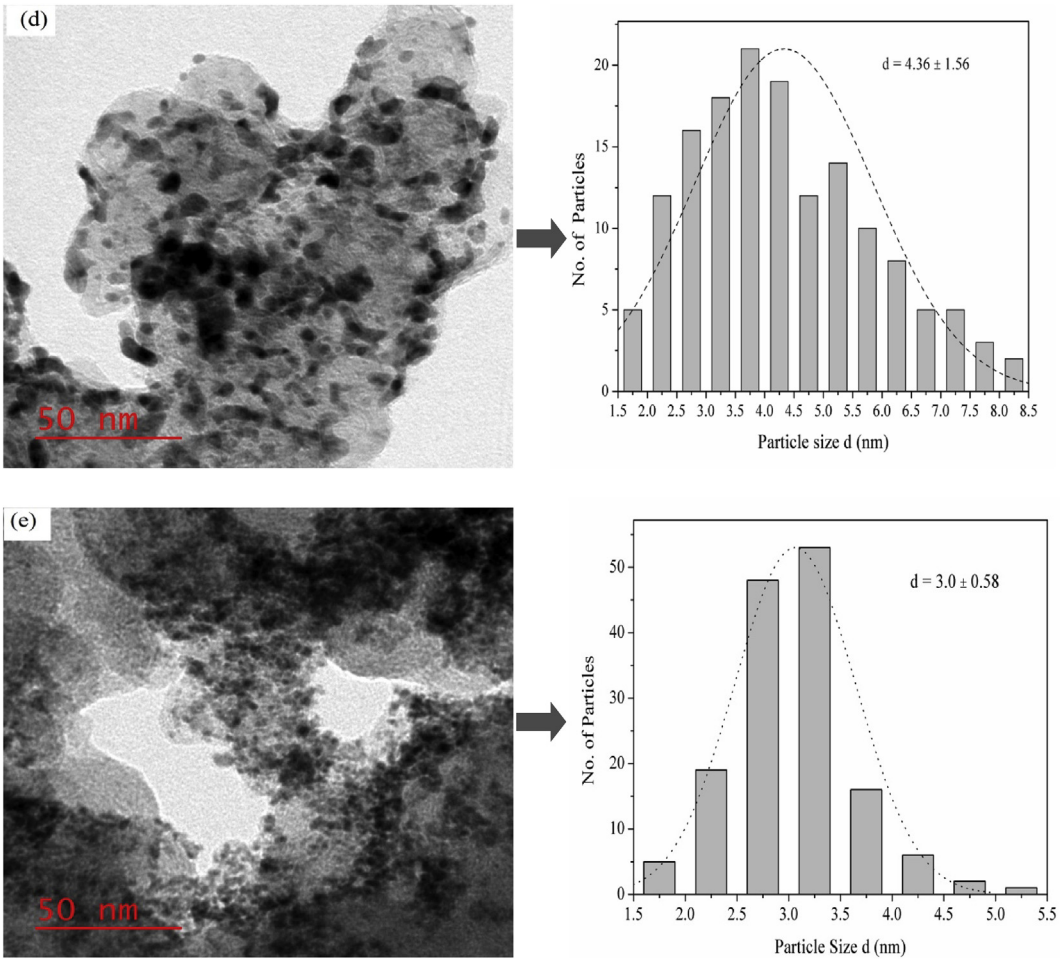

Fig. 5 – *(continued)*.

electrocatalyst Pt-Ru/C_{AB}-H_2-RT. However, the average particle size of Pt-Ru/C_{AB}-Air-160 (4.06 ± 1.13 nm) and Pt-Ru/C_{AB}-H_2-160 (4.36 ± 1.56 nm) are larger than Pt-Ru/C_{AB}-H_2-RT and commercial Pt-Ru/C electrocatalysts, respectively. The size distribution ranges are also wider for Pt-Ru/C_{AB}-Air-160 (1.5 nm–7.0 nm) and Pt-Ru/C_{AB}-H_2-160 (1.5 nm–8.5 nm) in comparison to Pt-Ru/C_{AB}-H_2-RT and commercial Pt-Ru/C electrocatalysts. The average particle sizes obtained from the TEM (Table 3) images agreed with the crystallite size values calculated from XRD measurements.

Table 3 – The average particle size of electrocatalysts from TEM analysis and comparison with XRD results.

Electrocatalysts	Average particle size (d_p) by TEM (nm)	Average crystallite size (d_c) by XRD (nm)
Pt-Ru/C_{AB}-syn	2.6 ± 0.35	–
Pt-Ru/C_{AB}-H_2-RT	3.3 ± 0.85	3.2
Pt-Ru/C_{AB}-Air-160	4.06 ± 1.13	3.5
Pt-Ru/C_{AB}-H_2-160	4.36 ± 1.56	3.8
Commercial Pt-Ru/C	3.0 ± 0.58	2.8

Selected area electron diffraction. The selected area electron diffraction (SAED) patterns of the electrocatalysts are presented in Fig. 6. The SAED patterns for the Pt-Ru/C_{AB}-syn (Fig. 6a) and commercial Pt-Ru/C (Fig. 6e) electrocatalysts show lower intensity of concentric fringes due to its lower crystallinity as explained in XRD section. The series of concentric rings together with some diffuse but distinct spots are assigned to hlk planes, which are characteristic of the Pt (fcc) crystal structure and consistence with the XRD results. The observed several sharp diffraction rings correspond to the (111), (200), (220), (311), and (222) planes of crystalline Pt (fcc) crystal structure. The first diffraction rings that represents the (002) plane of crystalline structure of carbon support.

Electrochemical evaluation of the synthesized electrocatalysts

Cyclic voltammetry (CV) measurements without ethanol

The surface characteristics of nanoparticles are very important since electrocatalytic reactions are sensitive to surface structures of electrocatalysts. Fig. 7 shows the base CV curves of all the electrocatalysts in nitrogen saturated supporting electrolyte of 0.5 M $HClO_4$ solution without ethanol at a temperature of 40 °C. The CVs profile of electrocatalysts revealed with two typical processes: hydrogen and oxygen

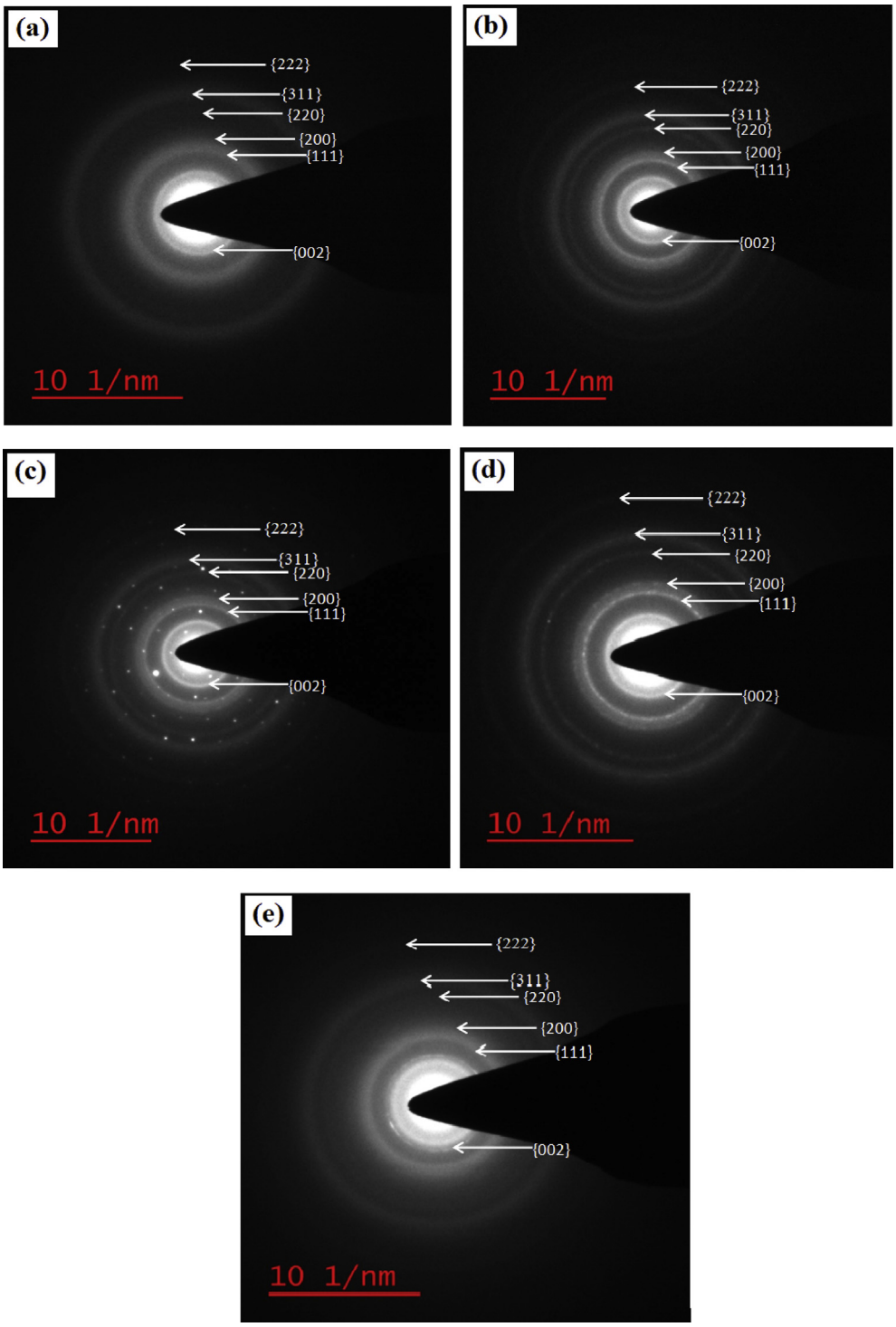

Fig. 6 – The SAED patterns of (a) Pt-Ru/C_{AB}-syn, (b) Pt-Ru/C_{AB}-H_2-RT, (c) Pt-Ru/C_{AB}-Air-160 and (d) Ru/C_{AB}-H_2-160 and (e) commercial Pt-Ru/C electrocatalysts.

adsorption/desorption regions. The hydrogen adsorption and desorption region of electrocatalysts in the range of −0.4 and 0.1 V, whereas oxygen adsorption/desorption of the electrocatalysts are 0.2–0.5 V. The polyol synthesized Pt-Ru/C_{AB}-syn show well defined hydrogen desorption peak at −0.18 V and this peak becomes prominent in the post treated electrocatalysts at higher temperatures. The hydrogen desorption peak at 0.2 V for commercial Pt-Ru/C is less prominent than post treated synthesized electrocatalysts. Moreover, the oxygen desorption peaks of the electrocatalysts are located at 0.2, 0.26, 0.36, 0.40 and 0.44 V for the commercial Pt-Ru/C, Ru/C_{AB}-H_2-160, Pt-Ru/C_{AB}-H_2-RT, Pt-Ru/C_{AB}-Air-160, and Pt-Ru/C_{AB}-syn electrocatalysts, respectively. The positive shift of oxygen desorption can be attributed to less Ru rich surface

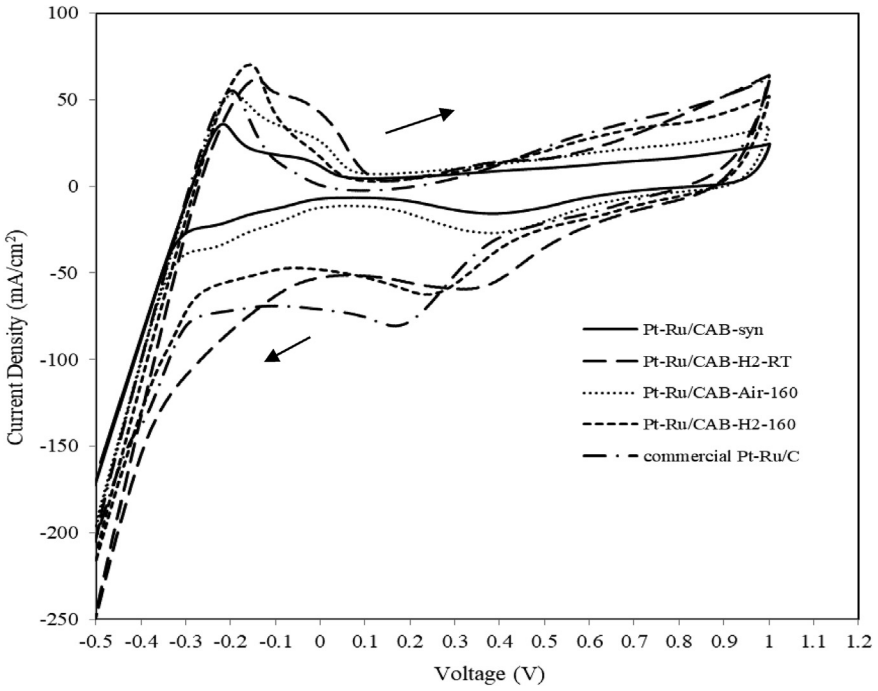

Fig. 7 – Cyclic voltammograms of synthesized Pt-Ru/C_{AB}-syn, Pt-Ru/C_{AB}-H_2-RT, Pt-Ru/C_{AB}-Air-160, Ru/C_{AB}-H_2-160 and commercial Pt-Ru/C electrocatalysts in 0.5 M $HClO_4$ without ethanol at a scan rate of 50 mVs^{-1} and temperature of 40 °C.

and or phase separation of Pt and Ru [44]. In addition, no peaks for ethanol electrooxidation were found in CVs of electrocatalysts in supporting electrolyte of 0.5 M $HClO_4$ aqueous solution.

Cyclic voltammetry (CV) measurement with ethanol

The ethanol electrooxidation activities of all the synthesized electrocatalysts were evaluated in cyclic voltammetry (CV) tests. Fig. 8 shows the CV curves of ethanol electrooxidation

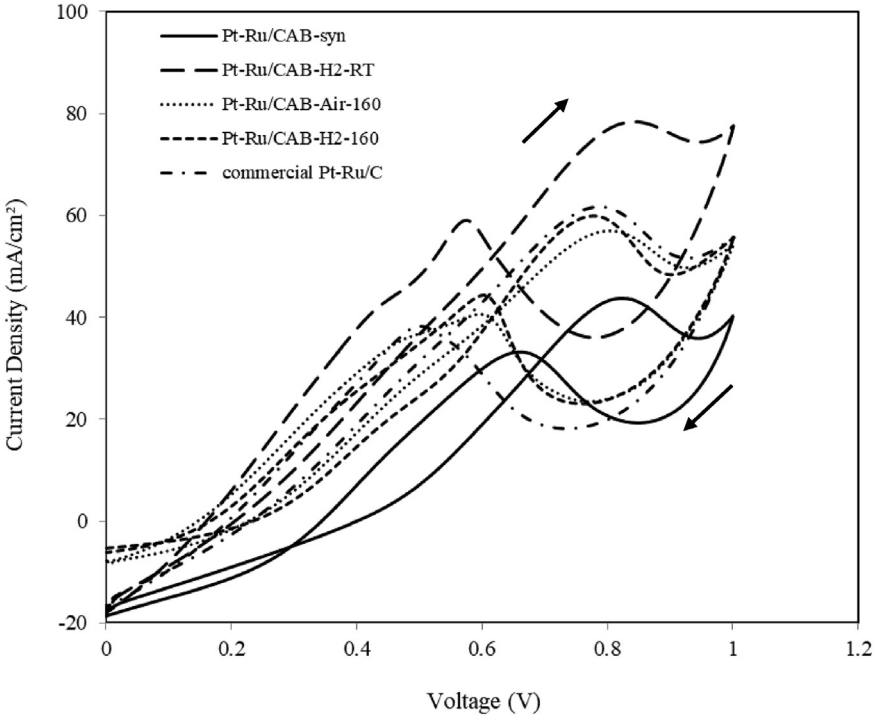

Fig. 8 – Cyclic voltammograms of synthesized Pt-Ru/C_{AB}-syn, Pt-Ru/C_{AB}-H_2-RT, Pt-Ru/C_{AB}-Air-160, Ru/C_{AB}-H_2-160 and commercial Pt-Ru/C electrocatalysts in 0.5 M $HClO_4$ containing 2 M ethanol with a scan rate of 20 mVs^{-1} and at a temperature of 40 °C.

on the polyol synthesized electrocatalysts in nitrogen saturated atmosphere in the potential range from 0 to 1.0 V using a uniform scan rate of 20 mVs^{-1}. It is seen from Fig. 8 that all the electrocatalysts resulting in a well-defined peak during the forward and backward scans as well.

The forward and reverse peak potentials and their corresponding current densities of ethanol electrooxidation on the synthesized and commercial electrocatalysts obtained by CV tests are summarized in Table 4. The synthesized electrocatalyst Pt-Ru/C_{AB}-H_2-RT gives the highest peak current density of 78.35 mA/cm^2 at a peak potential of 0.845 V. Moreover, during the reverse scan of the same electrocatalyst also produced the highest peak current density of 59.08 mA/cm^2 at a peak potential of 0.576 V.

On the other hand, peak current density of 61.60 mA/cm^2 at a peak potential of 0.796 V was obtained for commercial Pt-Ru/C electrocatalyst. Although, peak potential for commercial Pt-Ru/C during reverse scan was less positive (0.52 V), the peak current density was lowest (37.50 mA/cm^2) of all synthesized post treated electrocatalysts. The anodic peaks during forward scan for Pt-Ru/C_{AB}-Air-160 and Pt-Ru/C_{AB}-H_2-160 electrocatalysts were appeared at about 0.808 V and 0.779 V, respectively. The forward scan anodic peak current densities were 56.95 mA/cm^2 and 59.90 mA/cm^2 for Ru/C_{AB}-Air-160 and Pt-Ru/C_{AB}-H_2-160 electrocatalysts, respectively. It should be noted that the peak current densities for fresh synthesized Pt-Ru/C_{AB}-syn without post treatment was lowest of all the electrocatalysts during forward scan (43.74 mA/cm^2) and reverse scan (33.20 mA/cm^2), respectively. The electrooxidation peak in the reverse scan is due to further oxidation of carbonaceous intermediates species formed on the electrode surface and near the vicinity of the electrode during the forward scan. As already mentioned, the synthesized Pt-Ru/C_{AB}-H_2-RT shows highest anodic peak current density of 78.35 mA/cm^2 and possesses the highest electrocatalytic activity among all the electrocatalysts. The physical characterizations also showed excellent properties for Pt-Ru/C_{AB}-H_2-RT electrocatalyst. The difference in the peak potentials and corresponding current densities are attributed to the surface composition particle size, particle size, defects and degree of alloying.

Chronoamperometry

The stability or rate of surface poisoning of electrocatalysts were evaluated by the chronoamperometry measurement tests at two different cell potentials i.e. 0.45 V and 0.80 V in a solution of 0.5 M $HClO_4$ and 2 M ethanol (Fig. 9a–b). The lower reference potential value of 0.45 V was selected, which corresponds to the working anode potential in DEFC operations [64]. The higher reference potential value of 0.8 V was chosen, since the average anodic electrooxidation potential for all the studied electrocatalysts in CV analysis (Fig. 8) was found very close to 0.8 V. It is seen from Fig. 9a–b that the currents for ethanol electrooxidation on the supported Pt-Ru electrocatalysts dropped sharply at the initial stage, followed by a slow decrease in the current density and then steady-state current were obtained after ~400 s. The sharp decrease in current value is due to diffusion effects or charging current and the gradual decrease to the poisoning of electrocatalysts due to the formation of intermediates during ethanol electrooxidation. It is observed that at a lower potential of 0.45 V (Fig. 9a), the current density for ethanol electrooxidation on Pt-Ru/C_{AB}-H_2-RT electrocatalyst is significantly higher than that of all the other electrocatalysts. Similarly, at the higher potential of 0.8 V (Fig. 9b), the electrooxidation current density on Pt-Ru/C_{AB}-H_2-RT synthesized electrocatalyst is always higher in comparison to the synthesized Pt-Ru/C_{AB}-syn, Pt-Ru/C_{AB}-Air-160, synthesized Pt-Ru/C_{AB}-H_2-160 and commercial Pt-Ru/C electrocatalysts. The residual current density for ethanol electrooxidation at a potential of 0.45 V for the synthesized Pt-Ru/C_{AB}-syn, Pt-Ru/C_{AB}-H_2-RT, Pt-Ru/C_{AB}-Air-160, Ru/C_{AB}-H_2-160 and commercial Pt-Ru/C electrocatalysts were 6.30 mA/cm^2, 32.50 mA/cm^2, 9.5 mA/cm^2, 21.47 mA/cm^2 and 22.91 mA/cm^2, respectively. Furthermore, at the higher potential of 0.8 V, the residual current density of 9.74 mA/cm^2, 44 mA/cm^2, 12.1 mA/cm^2, 25.70 mA/cm^2 and 31 mA/cm^2 were obtained for ethanol electrooxidation using the synthesized Pt-Ru/C_{AB}-syn, Pt-Ru/C_{AB}-H_2-RT, Pt-Ru/C_{AB}-Air-160, Ru/C_{AB}-H_2-160 and commercial Pt-Ru/C electrocatalysts, respectively.

The synthesized Pt-Ru/C_{AB}-H_2-RT shows the superior performance in terms of current density for the tested time period at both electrode potentials of 0.45 V and 0.8 V. This can be attributed to the synergic effect of alloyed Ru and internal microstructure. The chronoamperometry studies also substantiate the results of CV (Fig. 8) obtained using synthesized and commercial electrocatalysts.

DEFC single cell performance

DEFC performance of anode electrocatalyst

Fig. 10 shows the polarization and power density characteristics of DEFC single cell using synthesized Pt-Ru/C_{AB}-syn, Pt-Ru/C_{AB}-H_2-RT, Pt-Ru/C_{AB}-Air-160d, Ru/C_{AB}-H_2-160d and commercial Pt-Ru/C electrocatalysts as anode of 1 mg/cm^2 loading in each electrode. The commercial Pt/C_{HSA} of 1 mg/cm^2 was used as cathode electrocatalyst.

Table 4 – CV results of synthesized Pt-Ru/C_{AB}-syn, Pt-Ru/C_{AB}-H_2-RT, Pt-Ru/C_{AB}-Air-160, Ru/C_{AB}-H_2-160 and commercial Pt-Ru/C electrocatalysts at 20 mV/s sweep rate for ethanol electrooxidation.

Anode electrocatalyst	Forward scan		Reverse scan	
	peak potential (V)	peak current density (mA/cm^2)	peak potential (V)	peak current density (mA/cm^2)
Pt-Ru/C_{AB}-syn	0.825	43.74	0.658	33.20
Pt-Ru/C_{AB}-H_2-RT	0.845	78.35	0.576	59.08
Pt-Ru/C_{AB}-Air-160	0.808	56.95	0.596	40.60
Pt-Ru/C_{AB}-H_2-160	0.779	59.90	0.60	44.31
commercial Pt-Ru/C	0.796	61.60	0.52	37.50

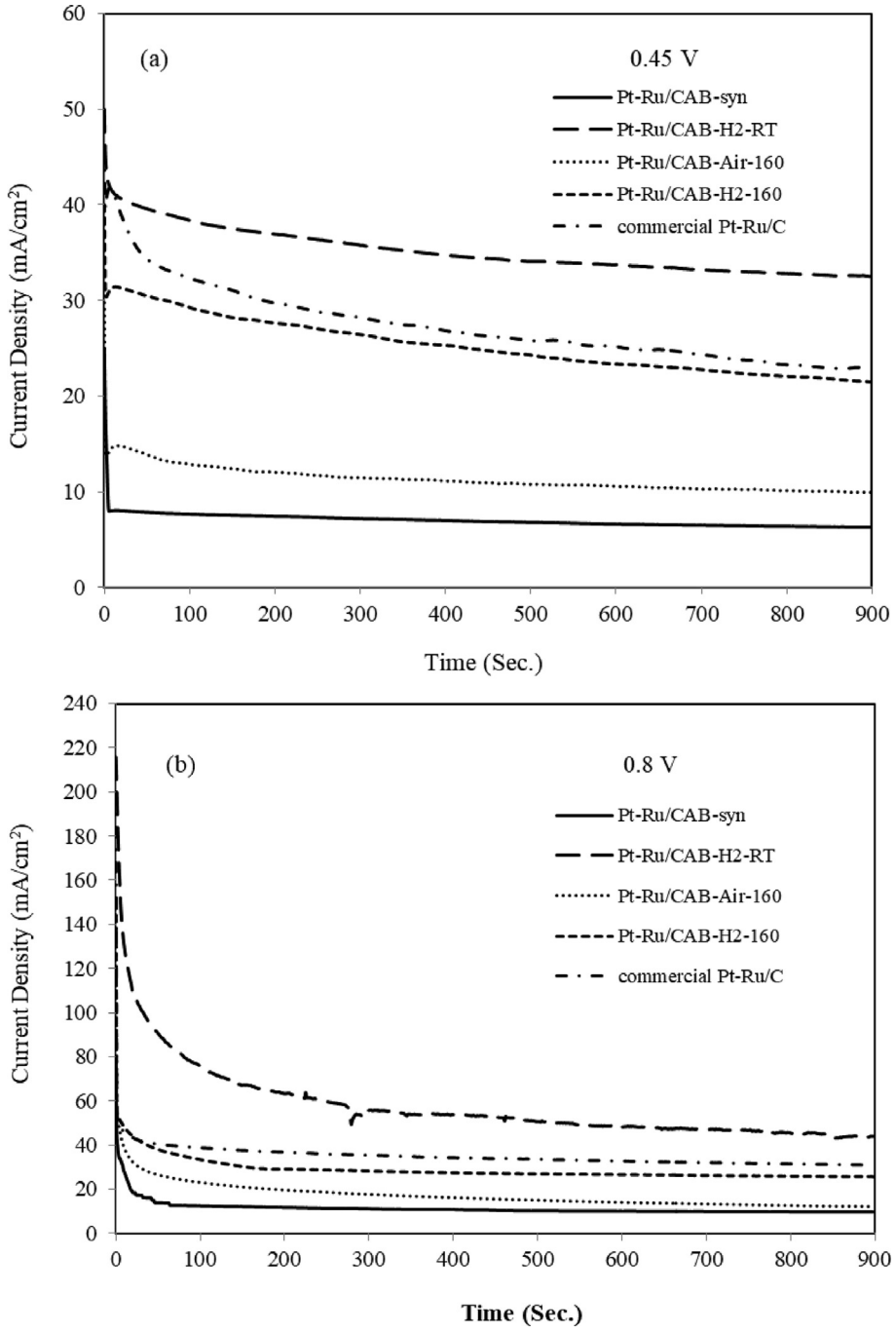

Fig. 9 – CA tests of ethanol oxidation in 0.5 M perchloric acid ($HClO_4$) containing 2 M ethanol solution on synthesized Pt-Ru/C_{AB}-syn, Pt-Ru/C_{AB}-H_2-RT, Pt-Ru/C_{AB}-Air-160, Ru/C_{AB}-H_2-160 and commercial Pt-Ru/C electrocatalysts at (a) 0.45 V vs. Ag/AgCl and (b) 0.8 V vs. Ag/AgCl at room temperature of 40 °C.

The electrolyte used was a commercial Nafion® 117 membrane. The DEFC temperature was kept similar to that of CV experiments performed i.e 40 °C. The maximum power density, current density at maximum power density and OCV of single cell output for various anode electrocatalysts are presented in Table 5.

It is seen from Fig. 10 that the synthesized Pt-Ru/C_{AB}-H_2-RT electrocatalyst resulting in open circuit voltage (OCV) of 0.718 V, which is near about same that of the commercial Pt-Ru/C (0.720 V) electrocatalyst. Whereas, the OCV for the synthesized Pt-Ru/C_{AB}-Air-160 and Pt-Ru/C_{AB}-H_2-160 electrocatalysts were 0.68 V and 0.712 V, those are lower than the commercial Pt-Ru/C electrocatalyst. The maximum power density of 9.15 mW/cm^2 at a current density of 32 mA/cm^2 and cell voltage of 0.286 V were obtained for synthesized Pt-Ru/C_{AB}-H_2-RT electrocatalyst, which is higher than that of all the other electrocatalysts. The best cell performance of synthesized Pt-Ru/C_{AB}-H_2-RT can be ascribed to the mild condition of

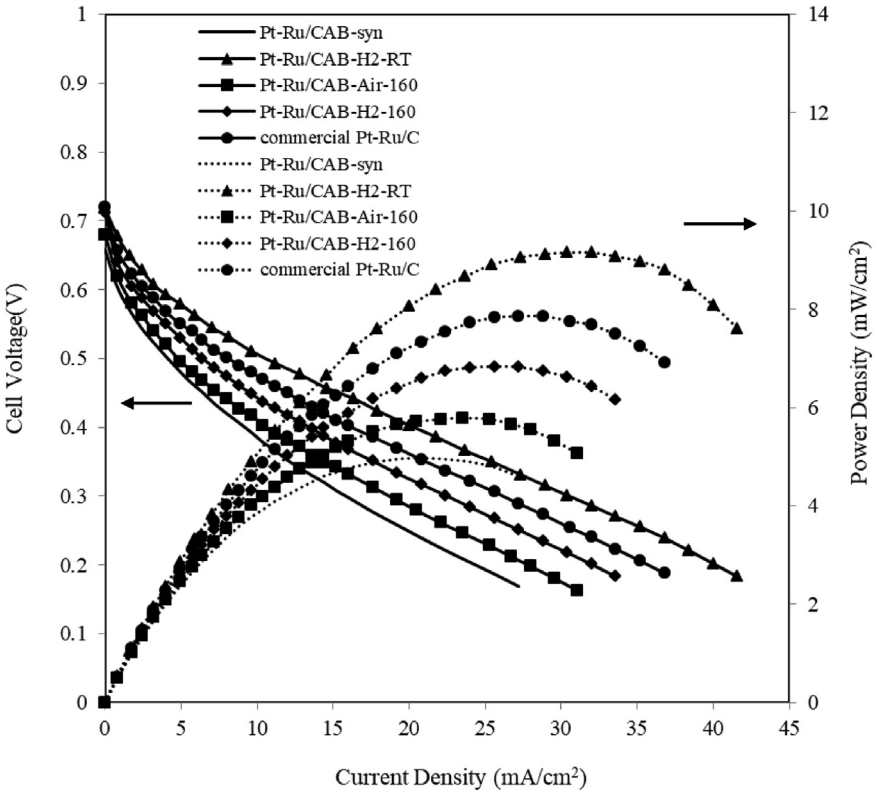

Fig. 10 – Polarization and power density curves for different synthesized electrocatalysts as anode with 1 mg/cm^2 electrocatalyst loading and cathode (commercial Pt/C_{HSA}) with 1 mg/cm^2 electrocatalyst loading at cell temperature of 40 °C. Anode: 2 M C_2H_5OH, 1.2 ml/min. Cathode: humidified oxygen, 60 ml/min. Solid electrolyte: Nafion® 117 membrane.

the post treatment so that the phase separation and agglomeration of metal nanoparticles are weak [38,44]. Whereas, the Pt-Ru/C_{AB}-Air-160 electrocatalyst resulted in the lowest OCV of 0.68 V and power density of 5.79 mW/cm^2 at a current density of 23.52 mA/cm^2 (Table 5). The single cell performance using as synthesized Pt-Ru/C_{AB}-syn electrocatalyst as an anode was lowest of all post treated and commercial electrocatalysts due to lower crystallinity and alloying degree of Ru. The reason for such poor performance of Pt-Ru/C_{AB}-syn has already been discussed in XRD section. It should be noted that CV and CA tests also showed highest activity for the synthesized Pt-Ru/C_{AB}-H_2-RT electrocatalyst as observed in the single cell study.

Table 5 – Summary of performance of synthesized Pt-Ru/C_{AB}-syn, Pt-Ru/C_{AB}-H_2-RT), Pt-Ru/C_{AB}-Air-160, Pt- Ru/C_{AB}-H_2-160 and commercial Pt-Ru/C electrocatalysts in single fuel cell tests for 2 M ethanol at a cell temperature of 40 °C.

Anode electrocatalysts	Open circuit Voltage (V)	Maximum power Density (mW/cm^2)	Current density at maximum power density (mA/cm^2)
Pt-Ru/C_{AB}-syn	0.658	4.97	20.8
Pt-Ru/C_{AB}-H_2-RT	0.718	9.15	32.0
Pt-Ru/C_{AB}-Air-160	0.68	5.79	23.52
Pt- Ru/C_{AB}-H_2-160	0.712	6.84	25.60
commercial Pt-Ru/C	0.720	7.86	28.80

Effect of cell temperature on synthesized Pt-Ru/C_{AB}-(H2-RT) electrocatalyst

Fig. 11 illustrates the effect of cell performance at various temperatures ranging from 40 °C to 80 °C for the synthesized best anode electrocatalyst Pt–Ru/C_{AB}-H_2-RT. The positive effect of temperature can be observed in terms of high current density and power density. The maximum power density of 9.15 mW/cm^2 at a cell voltage of 0.286 V and current density of 32 mA/cm^2 were achieved at the cell temperature of 40 °C. The DEFC power density reached at 16.23 mW/cm^2 at a cell voltage of 0.317 V and current density of 51.2 mA/cm^2 when cell temperature was increased to 80 °C. There was almost 77.4% increase in power density for the rise of cell temperature of 40 °C. The effect of temperatures on single DEFC's open circuit voltage and cell performance are summarized in Table 6. The enhanced performance accompanied with increment in cell operating temperatures can be attributed to the combined effect of a reduction of activation overpotential and ohmic polarization. The electrocatalytic activity of synthesized Pt-Ru/C_{AB}-H_2-RT for ethanol electrooxidation increases with the increase in cell temperature, thereby increasing current density [65–67]. Furthermore, high cell temperature enhances the proton conductivity of Nafion® membrane and Nafion® ionomer in the electrocatalyst layers, therefore ohmic polarization get reduced [66].

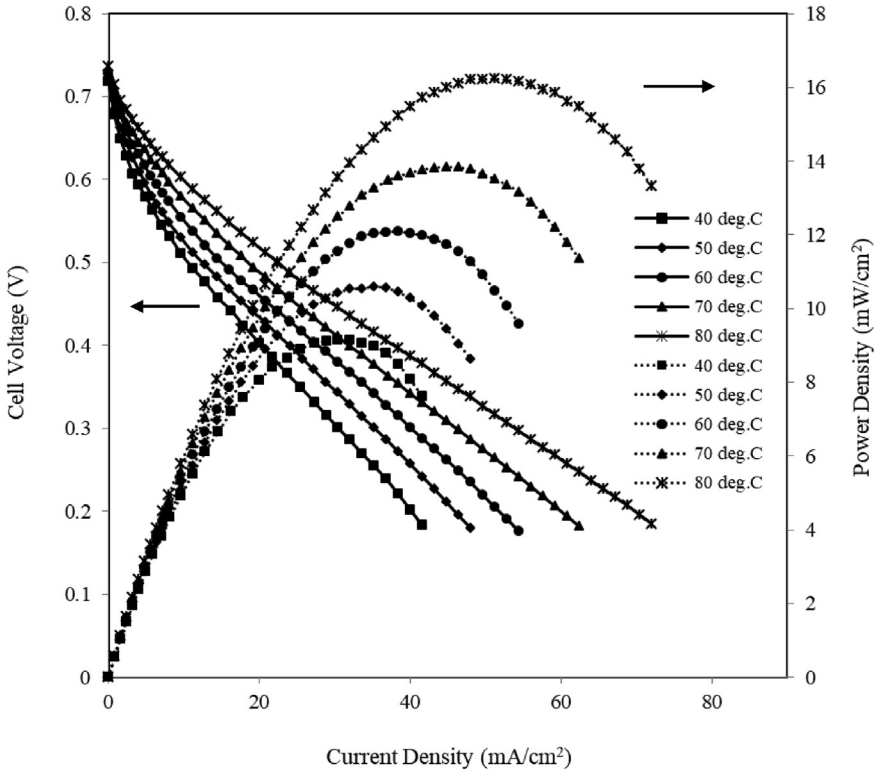

Fig. 11 – Performance curves of the synthesized Pt–Ru/C_{AB}-H_2-RT electrocatalyst with 1 mg/cm^2 electrocatalyst loading in anode side and the commercial Pt/C_{HSA} electrocatalyst as cathode with 1 mg/cm^2 electrocatalyst loading at various temperatures. Anode: 2 M ethanol, 1.2 ml/min flow rate. Cathode: humidified oxygen, 60 ml/min. Solid electrolyte: Nafion® 117 membrane.

Performance comparison with other Pt-Ru/C electrocatalysts in the literature

The cell performance using synthesized Pt-Ru/C_{AB}-H_2-RT electrocatalyst as anode is comparable with the cell performance reported in published literature (Table 7). Liu et al. [35] reported the performance DEFC using microwave-assisted polyol process synthesized Pt-Ru/C electrocatalyst in the anode at a cell temperature of 80 °C. The maximum OCV of ~0.85 V and power density ~60 mW/cm^2 were obtained. Although, cell performance was high, electrocatalyst loading at anode and cathode were 3 mg Pt/cm^2 and 2 mg Pt/cm^2, respectively, which is higher than our present study. In our present study synthesized Pt-Ru/C_{AB}-H_2-RT as anode electrocatalyst resulting in maximum OCV of 0.737 V and power density of 16.23 mW/cm^2 using anode and cathode electrocatalyst loading of 1 mg/cm^2 in both electrodes at a cell temperature of 80 °C. Pramanik et al. [67] studied on electrooxidation of ethanol using commercial Pt-Ru/C electrocatalyst in the anode and synthesized Nafion® 117 membrane at 90 °C for the anode and 60 °C for the cathode. The maximum OCV of 0.815 V and power density of 10.30 mW/cm^2 were obtained. The cell performance in our present study exhibits a maximum peak power density 1.58 times higher than obtained by Pramanik et al. Goel and Basu [19] reported an OCV of 0.61 V and peak power density of 17.50 mW/cm^2 using Pt-Ru/C electrocatalyst with 2 mg/cm^2 electrocatalyst loading at 100 °C. The peak power density is slightly higher than our present study and it may be due to high cell temperature (100 °C). This comparative study shows that synthesized post treated Pt-Ru/C_{AB}-H_2-RT synthesized by modified polyol method using C_{AB} as support material exhibits enhanced cell performance for the electrooxidation of ethanol as seen in the Table 7.

Table 6 – Summary of performance of synthesized Pt-Ru/C_{AB}-H_2-RT electrocatalysts in single fuel cell tests for 2 M ethanol at different operating cell temperature.

Electrocatalyst	Temperature (°C)	Open circuit Voltage (V)	Maximum power density (mW/cm^2)	Current density at maximum power density (mA/cm^2)
Pt-Ru/C_{AB}-H_2-RT	40	0.718	9.15	32.0
	50	0.723	10.60	35.2
	60	0.728	12.10	38.4
	70	0.732	13.84	44.8
	80	0.737	16.23	51.2

Table 7 – Single DEFC MEA performance comparison of laboratory synthesized electrocatalyst in the literature with Pt-Ru/C electrocatalysts using Nafion membrane in acidic media.

References	Type of membrane, electrocatalyst and loading	Other operating conditions	Maximum power density (mW/cm^2)	OCV (V)
Present Work	Nafion® 117; Anode: Pt-Ru/C_{AB}-H_2-RT (40 wt %, Pt:Ru = 1:1) (1 mg/cm^2), Cathode: Pt/C (40 wt %) (1 mg/cm^2) (AA*)	Fuel: ethanol (2 M) (1.2 ml/min); Oxidant: humidified O_2 (60 ml/min); Temperature: 80 °C	16.23	0.737
Liu et al. [35]	Nafion® 117; Anode: Pt-Ru/C (20 wt %, Pt:Ru = 1:1) (3 mg Pt/cm^2); Cathode: Pt/C (40 wt %, E-TEK) (2 mg Pt/cm^2)	Fuel: ethanol (2 M) (2 ml/min); Oxidant: humidified O_2 (500 cm^3/min); Temperature: 80 °C	~60.0	~0.85
Pramanik et al. [67]	Syn. Nafion® 117; Anode: Pt-Ru/C (40%:20% by wt., JM*) (1 mg/cm^2); Cathode: Pt black-HSA (JM*) (1 mg/cm^2)	Fuel: ethanol (2 M) (1.2 ml/min); Oxidant: O_2; Temperature: 90 °C	10.30	0.815
Goel and Basu [19]	Nafion® 117; Anode: Pt-Ru (40 wt %, Pt:Ru = 1:1)/C (2.0 mg/cm^2); Cathode: Pt/C (40 wt %, JM*) (1.0 mg/cm^2)	Fuel: ethanol (2 M) (1.0 ml/min); Oxidant: humidified (160 SCCM/min); Temperature: 100 °C	17.50	0.610

*JM-Johnson Matthey, AA-Alfa Aesar.

Conclusions

A low cost functionalized acetylene black carbon (C_{AB}) supported Pt-Ru/C_{AB}-RT was successfully synthesized and tested in DEFC which resulting in excellent performance in terms of power density and current density at low loading of Pt-Ru/C_{AB}-RT electrocatalyst. The post treatment of synthesized electrocatalyst under H_2 flow at room temperature improved the surface morphology, alloying degree and surface composition of Pt-Ru/C_{AB}-H_2-RT and performed as best electrocatalyst in this study. The modified surface composition and microstructures can be attributed to interconnection and the phase separation of metal nanoparticles such as Pt and Ru under H_2 flow at room temperature. The EDX and XRD analysis revealed the formation of carbon supported Pt-Ru bimetallic nano electrocatalysts having the typical fcc Pt crystalline structure and the formation of Pt-Ru alloy. The TEM and SEM analysis of electrocatalyst indicate that the metal nanoparticles are homogeneously dispersed with a size range of 1.5–6 nm on the surface of functionalized carbon nano support for the Pt-Ru/C_{AB}-H_2-RT electrocatalyst and was very similar to commercial Pt-Ru/C (1.5–5 nm) electrocatalyst. The most active synthesized Pt-Ru/C_{AB}-H_2-RT electrocatalyst yielded a maximum power density of 9.15 mW/cm^2, which is higher than that of commercial Pt-Ru/C (7.86 mW/cm^2) electrocatalyst at a temperature of 40 °C. The maximum power density of 16.23 mW/cm^2 at 0.317 V with a current density of 51.2 mA/cm^2 was obtained using Pt-Ru/C_{AB}-H_2-RT electrocatalyst as anode at a cell temperature of 80 °C. The electrochemical measurement tests and DEFC single cell performance tests showed that well alloyed synthesized Pt-Ru/C_{AB}-H_2-RT had a greater electrocatalytic activity for ethanol electrooxidation than the low alloyed synthesized Pt-Ru/C_{AB}-Air-160, Pt- Ru/C_{AB}-H_2-160 electrocatalyst by modified polyol method. The performance of Pt-Ru/C_{AB}-H_2-RT electrocatalyst synthesized by modified polyol method followed by post treatment indicates that the developed electrocatalyst has potential to be used as commercial electrocatalyst which might be available at low cost and recommended for moderate temperature DEFC.

Appendix A. Supplementary data

Supplementary data to this article can be found online at https://doi.org/10.1016/j.ijhydene.2019.10.243.

REFERENCES

[1] Shukla AK, Jackson CL, Scott K. The promise of fuel-based automobiles. Bull Mater Sci 2003;26:207–14.
[2] Lamy C, Lima A, LeRuhn V, Delime F, Coutanceau C, Leger JM. Recent advances in the development of direct alcohol fuel cells (DAFC). J Power Sources 2002;105:283–96.
[3] Olu PY, Job N, Chatenet M. Evaluation of anode (electro) catalytic materials for the direct borohydride fuel cell: methods and benchmarks. J Power Sources 2016;327:235–57.
[4] You PY, Kamarudin SK. Recent progress of carbonaceous materials in fuel cell applications: an overview. Chem Eng J 2017;309:489–502.
[5] Gupta UK, Pramanik H. Electrooxidation study of pure ethanol/methanol and their mixture for the application in direct alcohol alkaline fuel cells (DAAFCs). Int J Hydrogen Energy 2019;44:421–35.
[6] Çögenli MS, Yurtcan AB. Catalytic activity, stability and impedance behavior of PtRu/C, PtPd/C and PtSn/C bimetallic catalysts toward methanol and formic acid oxidation. Int J Hydrogen Energy 2018;43:10698–709.
[7] Antoniassi RM, Silva JC, Lopes T, Neto AO, Spinacé EV. Carbon-supported Pt nanoparticles with (100) preferential

orientation with enhanced electrocatalytic properties for carbon monoxide, methanol and ethanol oxidation in acidic medium. Int J Hydrogen Energy 2017;42:28786–96.
[8] Pramanik H, Basu S. A study on process parameters of direct ethanol fuel cell. Can J Chem Eng 2007;85:781–5.
[9] Teran FE, Santos DM, Ribeiro J, Kokoh KB. Activity of PtSnRh/C nanoparticles for the electrooxidation of C1 and C2 alcohols. Thin Solid Films 2012;520:5846–50.
[10] García G, Tsiouvaras N, Pastor E, Pena MA, Fierro JL, Martínez-Huerta MV. Ethanol oxidation on PtRuMo/C catalysts: in situ FTIR spectroscopy and DEMS studies. Int J Hydrogen Energy 2012;37:7131–40.
[11] Wang P, Wen Y, Yin S, Wang N, Shen PK. PtRh alloys on hybrid TiO_2–Carbon support as high efficiency catalyst for ethanol oxidation. Int J Hydrogen Energy 2017;42:24689–96.
[12] Ermete A. Catalysts for direct ethanol fuel cells. J Power Sources 2007;170:1–12.
[13] Nakagawa N, Kaneda Y, Wagatsuma M, Tsujiguchi T. Product distribution and the reaction kinetics at the anode of direct ethanol fuel cell with Pt/C, PtRu/C, and PtRuRh/C. J Power Sources 2012;199:103–9.
[14] Colmati F, Antolini E, Gonzalez ER. Effect of temperature on the mechanism of ethanol oxidation on carbon supported Pt, PtRu and Pt_3Sn electrocatalysts. J Power Sources 2006;2006(157):98–103.
[15] Hitmi H, Belgsir EM, Leger JM, Lamy C, Lezna RO. A kinetic analysis of the electro-oxidation of ethanol at a platinum electrode in acid medium. Electrochim Acta 1994;39:407–15.
[16] Pramanik H, Basu S. Modeling and experimental validation of overpotentials of a direct ethanol fuel cell. Chem Eng Process Process Intensif 2010;49:635–42.
[17] Goel J, Basu S. Mathematical modeling and experimental validation of direct ethanol fuel cell. Int J Hydrogen Energy 2015;40:14405–15.
[18] Antolini E. Effect of the structural characteristics of binary Pt–Ru and ternary Pt–Ru–M fuel cell catalysts on the activity of ethanol electrooxidation in acid medium. ChemSusChem 2013;6:966–73.
[19] Goel J, Basu S. Effect of support materials on the performance of direct ethanol fuel cell anode catalyst. Int J Hydrogen Energy 2014;39:15956–66.
[20] Song SQ, Zhou WJ, Zhou ZH, Jiang LH, Sun GQ, Xin Q, et al. Direct ethanol PEM fuel cells: the case of platinum based anodes. Int J Hydrogen Energy 2005;30:995–1001.
[21] Li H, Sun G, Cao L, Jiang L, Xin Q. Comparison of different promotion effect of PtRu/C and PtSn/C electrocatalysts for ethanol electro-oxidation. Electrochim Acta 2007;52:6622–9.
[22] Colmenares L, Wang H, Jusys Z, Jiang L, Yan S, Sun GQ, Behm RJ. Ethanol oxidation on novel, carbon supported Pt alloy catalysts—Model studies under defined diffusion conditions. Electrochim Acta 2006;52:221–33.
[23] Tayal J, Rawat B, Basu S. Bi-metallic and tri-metallic Pt-Sn/C, Pt-Ir/C, Pt-Ir-Sn/C catalysts for electro-oxidation of ethanol in direct ethanol fuel cell. Int J Hydrogen Energy 2011;36:14884–97.
[24] Tayal J, Rawat B, Basu S. Effect of addition of rhenium to Pt-based anode catalysts in electro-oxidation of ethanol in direct ethanol PEM fuel cell. Int J Hydrogen Energy 2012;37:4597–605.
[25] Silva-Junior LC, Maia G, Passos RR, de Souza EA, Camara GA, Giz MJ. Analysis of the selectivity of PtRh/C and PtRhSn/C to the formation of CO_2 during ethanol electrooxidation. Electrochim Acta 2013;112:612–9.
[26] Herrera-Méndez HD, Roquero P, Smit MA, Ordóñez LC. Carbon-supported platinum molybdenum electro-catalysts and their electro-activity toward ethanol oxidation. Int J Electrochem Sci 2011;6:4454–69.
[27] Pech-Rodríguez WJ, González-Quijano D, Vargas-Gutiérrez G, Morais C, Napporn TW, Rodríguez-Varela FJ. Electrochemical and in situ FTIR study of the ethanol oxidation reaction on PtMo/C nanomaterials in alkaline media. Appl Catal B Environ 2017;203:654–62.
[28] Datta J, Singh S, Das S, Bandyopadhyay NR. A comprehensive study on the effect of Ru addition to Pt electrodes for direct ethanol fuel cell. Bull Mater Sci 2009;32:643–52.
[29] Gu Z, Li S, Xiong Z, Xu H, Gao F, Du Y. Rapid synthesis of platinum-ruthenium bimetallic nanoparticles dispersed on carbon support as improved electrocatalysts for ethanol oxidation. J Colloid Interface Sci 2018;521:111–8.
[30] Liu P, Logadottir A, Nørskov JK. Modeling the electro-oxidation of CO and H_2/CO on Pt, Ru, PtRu and Pt3Sn. Electrochim Acta 2003;48:3731–42.
[31] Velázquez-Palenzuela A, Centellas F, Garrido JA, Arias C, Maria Rodriguez R, Brillas E, et al. Structural properties of unsupported Pt–Ru nanoparticles as anodic catalyst for proton exchange membrane fuel cells. J Phys Chem C 2010;114:4399–407.
[32] Samad S, Loh KS, Wong WY, Lee TK, Sunarso J, Chong ST, et al. Carbon and non-carbon support materials for platinum-based catalysts in fuel cells. Int J Hydrogen Energy 2018;43:7823–54.
[33] Lázaro MJ, Celorrio V, Calvillo L, Pastor E, Moliner R. Influence of the synthesis method on the properties of Pt catalysts supported on carbon nanocoils for ethanol oxidation. J Power Sources 2011;196:4236–41.
[34] Calvillo L, Celorrio V, Moliner R, Lázaro MJ. Influence of the support on the physicochemical properties of Pt electrocatalysts: comparison of catalysts supported on different carbon materials. Mater Chem Phys 2011;127:335–41.
[35] Liu Z, Ling XY, Su X, Lee JY, Gan LM. Preparation and characterization of Pt/C and PtRu/C electrocatalysts for direct ethanol fuel cells. J Power Sources 2005;149:1–7.
[36] Esmaeilifar A, Rowshanzamir S, Eikani MH, Ghazanfari E. Synthesis methods of low-Pt-loading electrocatalysts for proton exchange membrane fuel cell systems. Energy 2010;35:3941–57.
[37] Asgardi J, Calderón JC, Alcaide F, Querejeta A, Calvillo L, Lázaro MJ, et al. Carbon monoxide and ethanol oxidation on PtSn supported catalysts: effect of the nature of the carbon support and Pt: Sn composition. Appl Catal B Environ 2015;168:33–41.
[38] Rizo R, Sebastián D, Rodríguez JL, Lázaro MJ, Pastor E. Influence of the nature of the carbon support on the activity of Pt/C catalysts for ethanol and carbon monoxide oxidation. J Catal 2017;348:22–8.
[39] Rizo R, Sebastián D, Lázaro MJ, Pastor E. On the design of Pt-Sn efficient catalyst for carbon monoxide and ethanol oxidation in acid and alkaline media. Appl Catal B Environ 2017;200:246–54.
[40] de La Fuente JG, Martínez-Huerta MV, Rojas S, Hernández-Fernández P, Terreros P, Fierro JL, et al. Tailoring and structure of PtRu nanoparticles supported on functionalized carbon for DMFC applications: new evidence of the hydrous ruthenium oxide phase. Appl Catal B Environ 2009;88:505–14.
[41] Pérez-Rodríguez S, Pastor E, Lázaro MJ. Electrochemical behavior of the carbon black Vulcan XC-72R: influence of the surface chemistry. Int J Hydrogen Energy 2018;43:7911–22.
[42] Bock C, Paquet C, Couillard M, Botton GA, MacDougall BR. Size-selected synthesis of PtRu nano-catalysts: reaction and size control mechanism. J Am Chem Soc 2004;126:8028–37.
[43] Wang G, Takeguchi T, Muhamad EN, Yamanaka T, Ueda W. Investigation of grain boundary formation in PtRu/C catalyst

obtained in a polyol process with post-treatment. Int J Hydrogen Energy 2011;36:3322–32.
[44] Lee KS, Park HY, Cho YH, Park IS, Yoo SJ, Sung YE. Modified polyol synthesis of PtRu/C for high metal loading and effect of post-treatment. J Power Sources 2010;195:1031–7.
[45] Zhiani M, Jalili J, Rezaei B, Taghiabadi MM. Methanol electrooxidation on synthesized PtRu nanocatalyst supported on acetylene black in half cell and in direct methanol fuel cell. Int J Hydrogen Energy 2013;38:5419–24.
[46] Choudhary AK, Pramanik H. Synthesis of low-cost HNO 3-functionalized acetylene black carbon supported Pt-Ru/C AB nano electrocatalysts for the application in direct ethanol fuel cell (DEFC). Korean J Chem Eng 2019;36:1688–707.
[47] Tang J, Yang J, Zhou X, Xie J, Chen G. Oxidation of acetylene black by nitric acid in hermetically sealed condition. Microporous Mesoporous Mater 2014;193:54–60.
[48] Lee WD, Lim DH, Chun HJ, Lee HI. Preparation of Pt nanoparticles on carbon support using modified polyol reduction for low-temperature fuel cells. Int J Hydrogen Energy 2012;37:12629–38.
[49] Zhiani M, Gasteiger HA, Piana M, Catanorchi S. Comparative study between platinum supported on carbon and non-noble metal cathode catalyst in alkaline direct ethanol fuel cell (ADEFC). Int J Hydrogen Energy 2011;36:5110–6.
[50] Higa M, Hatemura K, Sugita M, Maesowa SI, Nishimura M, Endo N. Performance of passive direct methanol fuel cell with poly (vinyl alcohol)-based polymer electrolyte membranes. Int J Hydrogen Energy 2012;37:6292–301.
[51] Fievet F, Lagier JP, Blin B, Beaudoin B, Figlarz M. Homogeneous and heterogeneous nucleations in the polyol process for the preparation of micron and submicron size metal particles. Solid State Ion 1989;32:198–205.
[52] Komarneni S, Li D, Newalkar B, Katsuki H, Bhalla AS. Microwave– polyol process for Pt and Ag nanoparticles. Langmuir 2002;18:5959–62.
[53] Yang J, Deivaraj TC, Too HP, Lee JY. Acetate stabilization of metal nanoparticles and its role in the preparation of metal nanoparticles in ethylene glycol. Langmuir 2004;20:4241–5.
[54] Wang Y, Zhang J, Wang X, Ren J, Zuo B, Tang Y. Metal nanoclusters stabilized with simple ions and solvents—promising building blocks for future catalysts. Top Catal 2005;35:35–41.
[55] Oh HS, Oh JG, Hong YG, Kim H. Investigation of carbon-supported Pt nanocatalyst preparation by the polyol process for fuel cell applications. Electrochim Acta 2007;52:7278–85.
[56] Chu YY, Wang ZB, Jiang ZZ, Gu DM, Yin GP. Effect of pH value on performance of PtRu/C catalyst prepared by microwave-assisted polyol process for methanol electrooxidation. Fuel Cells 2010;10:914–9.
[57] Hu Y, Zhu A, Zhang Q, Liu Q. Preparation of PtRu/C core–shell catalyst with polyol method for alcohol oxidation. Int J Hydrogen Energy 2016;41:11359–68.
[58] Pires FI, Corradini PG, Paganin VA, Antolini E, Perez J. Effect of the degree of alloying of PtRu/C (1: 1) catalysts on ethanol oxidation. Ionics 2013;19:1037–45.
[59] Antolini E, Cardellini F. Formation of carbon supported PtRu alloys: an XRD analysis. J Alloys Comp 2001;315:118–22.
[60] Guo J, Sun G, Shiguo S, Shiyou Y, Weiqian Y, Jing Q, Yushan Y, Qin X. Polyol-synthesized PtRu/C and PtRu black for direct methanol fuel cells. J Power Sources 2007;168:299–306.
[61] dos Santos L, Colmati F, Gonzalez ER. Preparation and characterization of supported Pt–Ru catalysts with a high Ru content. J Power Sources 2006;159:869–77.
[62] Yang B, Lu Q, Wang Y, Zhuang L, Lu J, Liu P, et al. Simple and low-cost preparation method for highly dispersed PtRu/C catalysts. Chem Mater 2003;15:3552–7.
[63] Qian Y, Wen W, Adcock PA, Jiang Z, Hakim N, Saha MS, et al. PtM/C catalyst prepared using reverse micelle method for oxygen reduction reaction in PEM fuel cells. J Phys Chem C 2008;112:1146–57.
[64] Roca-Ayats M, García G, Soler-Vicedo M, Pastor E, Lázaro MJ, Martínez-Huerta MV. The role of Sn, Ru and Ir on the ethanol electrooxidation on Pt_3M/TiCN electrocatalysts. Int J Hydrogen Energy 2015;40:14519–28.
[65] Song S, Zhou W, Tian J, Cai R, Sun G, Xin Q, et al. Ethanol crossover phenomena and its influence on the performance of DEFC. J Power Sources 2005;145:266–71.
[66] Alzate V, Fatih K, Wang H. Effect of operating parameters and anode diffusion layer on the direct ethanol fuel cell performance. J Power Sources 2011;196:10625–31.
[67] Pramanik H, Wragg AA, Basu S. Studies of some operating parameters and cyclic voltammetry for a direct ethanol fuel cell. J Appl Electrochem 2008;38:1321–8.